Spectral methods in general relativistic astrophysics

S. Bonazzola, E. Gourgoulhon & J.-A. Marck

Département d'Astrophysique Relativiste et de Cosmologie,
(UPR 176 du C.N.R.S.),
Observatoire de Paris, Section de Meudon,
F-92195 Meudon Cedex, France
e-mail : Silvano.Bonazzola,Eric.Gourgoulhon,Jean-Alain.Marck@obspm.fr

Abstract

We present spectral methods developed in our group to solve three-dimensional partial differential equations. The emphasis is put on equations arising from astrophysical problems in the framework of general relativity.

1 Introduction

Astrophysical problems involve many field of physics: hydrodynamics, magneto hydrodynamics, chemistry, kinetical, nuclear and statistical physics, gravitation... Physicists and astrophysicists have developed well suited techniques to solve numerically mathematical problems in each of these specific fields. Moreover they have to handle problems in which different branches of physics interact and therefore compatibility of different numerical techniques is required.

The following examples illustrate the above statement. Chaotic chemical reactions can occur in the interstellar medium [34]. Moreover the interstellar medium is turbulent and mildly supersonic. Therefore the numerical modelizations requires numerical methods able to describe chaos *and* compressible turbulence. Astrophysicists involved in numerical work are confronted with problems that require the integration of systems of quasi-linear partial differential equations (PDEs) (i.e. PDEs which are linear in the highest order derivatives). In general these systems of equations contain all kind of PDEs *i.e.* hyperbolic, parabolic and elliptic PDEs. The study of stellar oscillations is another good example. The system of PDEs that must be integrated is the Navier-Stokes equation for the fluid motion coupled to the continuity equation

for the mass conservation, to the scalar Poisson equation for the gravitational field and to the heat equation (since the plasma of the star has a finite heat conductivity).

PDEs systems for special relativistic astrophysics present the same structure than the Newtonian ones but special relativistic hydrodynamic equations are more complicated because of the presence of high Lorentz factors which make life less easy. Relativistic jets in active galactic nuclei are the realm of special relativistic [magneto-] hydrodynamics codes. Things change drastically for compact astrophysical objects such as neutron stars and black holes. For these objects the Newtonian theory of the gravitation is no longer appropriate and general relativity must be used.

Differential geometry is the realm of GR. New geometrical concepts such as topology, globality, isometry, Lie derivative, Killing vector, curvature, etc... play an essential role. Of course all these concepts are present in the framework of special relativity, but in a trivial and underlying way. Therefore, astrophysicists dealing with special relativity, as a modern Monsieur Jourdain who *"fait de la prose sans le savoir"* (he speaks in prose without knowing it), use these concepts without realizing it.

In general relativity, the gravitational potential is no longer scalar. The metric tensor $g_{\alpha\beta}$, $(\alpha, \beta = 0, 1, 2, 3)$ replaces it, its 10 independent components playing the role of gravitational potentials. The gravitational field equations (Einstein equations) can be written in a beautiful very compact form:

$$R_{\alpha\beta} - \frac{1}{2} R g_{\alpha\beta} = \frac{8\pi G}{c^4} T_{\alpha\beta} \ , \tag{1}$$

where $R_{\alpha\beta} = R_{\beta\alpha}$ and R are respectively the Ricci tensor and the curvature scalar $R = R^{\alpha}{}_{\alpha}$ associated with the metric $g_{\alpha\beta}$, and where $T_{\alpha\beta}$ is the energy-momentum tensor. The equations of motion can be written in a compact way too : $\nabla_{\alpha} T^{\alpha}{}_{\beta} = 0$. If an electromagnetic field is present, the Maxwell equations must be added to the above equations : $\nabla_{\alpha} F^{\alpha}{}_{\beta} = J_{\beta}$ where $F^{\alpha}{}_{\beta}$ is the electromagnetic tensor and J_{β} is the quadri-electric current. The simplicity of these equations is only apparent. In fact, when explicited, they contain a few thousand of terms. Finding a solution to a complete 3-D physical problem in the framework of general relativity is the *Holly Grail* of Numerical Relativity.

Einstein equations form a system of 10 second order quasi-linear PDEs. Moreover, the 4 identities (Bianchi identities)

$$\nabla_{\alpha} (R^{\alpha}{}_{\beta} - \frac{1}{2} R g^{\alpha}{}_{\beta}) \equiv 0 \tag{2}$$

introduce 4 degrees of freedom for the solution. This is equivalent to the free-

dom of gauge choice in electromagnetism. The choice of the gauge in GR defines the character (i.e. ellipticity, parabolicity or hyperbolicity) of the equations. Actually, the Einstein's equations are degenerated in the sense that their character depends on the gauge choice. For example, these equations are all hyperbolic when the so-called *harmonic gauge* [1] is chosen and, on the contrary, the system can be reduced to 5 elliptic equations coupled to 5 hyperbolic equations if the so-called *radiation gauge* [53] is chosen.

The first problem which arises naturally when one wants to solve the Einstein equation for a particular astrophysical problem is the determination of the most appropriate gauge. There is no definitive answer to this question and the debate is still open. One has to consider essentially two criteria. The first one depends on the physics of the problem: depending on the coordinate system the space-time slicing induced by the gauge may or may not be able to describe and cover the physical event that one wants to study. The second one depends on the numerical technique employed: depending on the gauge one may or may not be able to find a numerical solution to the equations (e.g. ability to solve coupled non-linear elliptic equations). It is tempting to choose a gauge which seems more appropriate to the numerical technique used. However, we don't think that this is a good approach to the problem.

We hope to have given to the reader a vague idea of the kind of problems met by astrophysicists and of the mathematical difficulties that have to be overcome. We will show in this paper how spectral methods may be used to successfully overcome these difficulties. Spectral methods (SM) will be introduced in details in Sect. 2. For now, let us anticipate two of the most important advantages of SM. The first one is the economy of the number of degrees of freedom (NDF). For a given numerical accuracy, less degrees of freedom are required than in the case of finite difference techniques. More precisely, as a rule of thumb, we can say that with SM, the number of grid points is reduced by a factor of five per space dimension. This means that, in the case of 3-D problems, the number of grid points will be decreased by a factor of $5^3 = 125$. Now, if one consider a dynamical problem where the integration time step scales at least as N, where N is the NDF, this advantage becomes obvious. The second advantage consists in the possibility of using a coordinate system well adapted to the geometry of the problem and to handle exactly the pseudo-singularities potentially present in the chosen coordinate system. For instance, thanks to SM it has been possible to study 3-D turbulent motion of an incompressible fluid with Reynolds number of about 1000 [55] and to describe the disruption of a star in the tidal field of a black hole in less than 3 hours of C.P.U. time on a workstation [39] when the same problem, using a finite difference method, has required 30 hours of C.P.U. time on a Cray-2 [32]. Moreover, thanks to the high precision achievable with SM the stability and collapse of a N.S. close to its critical mass was successfully studied in the GR frame [22], [26].

Elliptic and parabolic PDEs are the realm of SM. Nevertheless good results can be obtained for hyperbolic equations too if no discontinuities appear in the solution [16], [39]. When a discontinuity is present, some kind of natural or artificial viscosity must be added in order to obtain a sufficiently smooth solution. Interesting results were obtained with this technique in describing a mildly supersonic turbulence occurring in star formation [15,48,54,49], or, by our group, in modelling a 3-D stellar collapse [37]. Other numerical methods (especially those based on Riemann solvers technique [40]) have been developed in order to handle shocks. Successful results were obtained in modelizing relativistic jets (see [31] and literature quoted there). In the case of relativistic problems where systems of elliptical coupled to hyperbolic PDEs must be solved, an interesting strategy consists in using SM for the elliptical equations and Riemann solver technique for the hyperbolic equations where discontinuities may occur. Interesting results have already been obtained in 1-D modellisation of the collapse of a core of a supernova in the framework of a tensor-scalar theory of gravitation [42], [43]. This strategy looks very promising too for 3-D problems.

Our aim in the present paper is to explain how SM work and how they can be implemented in the easiest way. The mathematical theory of SM will be left to specialized literature (e.g. [21], [18]). The reader does not need to know astrophysics but almost all the examples presented as illustration are taken from the modelization of astrophysical phenomena. Therefore some short explanation of the phenomenon that has motivated the modelization will be given. On the contrary some elementary notions of differential geometry would be worth for understanding the mathematical problems.

The plan of this paper is as follows. We give first a short introduction to spectral methods (Sect. 2) in which the essential notions are presented. Then we explicit the algebraic properties of representation of some relevant differential operators (Sect. 3). Basic methods for solving PDEs are presented in Sect. 4, especially the time scheme and the treatment of boundary conditions. This is illustrated by selected one-dimensional examples (Sect. 5). Three-dimensional (3-D) spectral methods with spherical-like coordinates are introduced in Sect. 6. Scalar and vectorial equations, such as Poisson or telegraph equations, are considered in Sects. 7 and 8 respectively. After a brief discussion of the structure of Einstein equations, the paper ends by the presentation of various astrophysical results (Sect. 9).

2 Introduction to spectral methods

2.1 A simple example based on a Fourier expansion

In this section we present the main ideas underlying spectral methods (SM). We shall give only the basic notions, living the theory to specialized and very good existing text books, among which we recommend the monographies by Gottlieb & Orzsag [21] and by Canuto, Hussaini Quarteroni & Zang [18].

Let us consider the quasi-linear partial differential equation (viscous Burger equation):

$$\frac{\partial u}{\partial t} = \frac{\partial^2 u}{\partial x^2} + \lambda u \frac{\partial u}{\partial x} \ , \quad t \geq 0 \ , \quad x \in [0,1] \ , \tag{3}$$

where u is a function of the two variables t and x and λ is some parameter.

Consider first the simple case $\lambda = 0$ (linear heat equation). Let us assume that the value of $u(t,x)$ is known for all x at $t = 0$ and that u is a periodic function. The basic idea underlying SM consists to transform the PDE in a system of ordinary differential equations by means of a expansion of the solution onto a series on a complete basis. Since u is assumed to be periodic, it is natural to use a Fourier expansion:

$$u(x,t) = \sum_{k=0}^{\infty} \left[a_k(t) \cos(2\pi k x) + b_k(t) \sin(2\pi k x) \right] \ . \tag{4}$$

Equation. (3), with $\lambda = 0$, can then be rewritten as

$$\frac{da_k}{dt} = -k^2 a_k(t) \ , \quad \frac{db_k}{dt} = -k^2 b_k(t) \ . \tag{5}$$

In this way, finding a solution of the PDE (3) turns out to be equivalent to solve the infinite system of ordinary differential equations (5), where the initial values of the coefficients a_k and b_k are given by the Fourier expansion of the function u at the time $t = 0$:

$$a_k(0) = \int_0^1 u(x,0) \cos(2\pi k x)\, dx, \qquad b_k(0) = \int_0^1 u(x,0) \sin(2\pi k x)\, dx \ . \tag{6}$$

From the numerical point of view, the series (4) has to be truncated. Let be $N/2 - 1$ the highest term of the series (N even). The integrals (6) must be evaluated numerically in the most accurate way: if $u(x,0)$ does not contain spatial frequencies higher than $N/2 - 1$, then its Fourier coefficients a_k and

b_k must be computed exactly within the roundoff errors. In other words we require that the numerical integrals

$$\int_0^1 \cos(2\pi kx)\cos(2\pi jx)dx \ , \int_0^1 \sin(2\pi kx)\sin(2\pi jx)dx \ ,$$
$$\int_0^1 \sin(2\pi kx)\cos(2\pi jx)dx \tag{7}$$

are computed exactly. The minimum number of grid points at which the functions $u(x,0)$ must be sampled is N. The sampling points that fulfil the above requirements are called the *Gauss-Lobatto points* or *collocation points*: $x_j = j/N$. These points are equally spaced [1] .

Note that there exists an isomorphism between the coefficients $a_k(t), b_k(t)$ and the values $u(x_j,t)$ of the function at the collocation points. For this reason, N is called the *number of degrees of freedom* (NDF), denomination that we prefer to the more usual *number of grid points*. Finally it is worth to note that the uniform repartition of the Gauss-Lobatto points should be considered as an accident. If one changes the basis of expansion, uniform spacing does not a priori correspond to a Gauss-Lobatto sampling (see the next section).

Consider now the non linear problem $\lambda \neq 0$. We can proceed in two different ways to treat the non-linear term. The first one (*spectral method* in the strict sense) consists in computing the first space derivative of u in the Fourier space (or coefficient space) and to perform a convolution with u_k. From a numerical point of view, these terms, computed at the time t^j, act as a source and allow to compute the coefficient u_k at the time t^{j+1} no matter the temporal scheme used. Within spectral method, all the evolution of the equation is computed in the Fourier space. Backing in the configuration space (at arbitrary values

[1] The properties of the Gauss-Lobatto sampling for the discrete Fourier decomposition can be recovered easily by bearing in mind that $\sum_{n=0}^{N-1} q^n = (1-q^N)/(1-q)$, $|q| \leq 1$, from which the following identity holds ($q = \exp(2\pi i(k-j)/N)$):

$$N\int_0^1 \exp(2i\pi(k-j)x)dx = \sum_{n=0}^{N-1} \exp(2i\pi(k-j)x_n)$$
$$= \sum_{n=0}^{N-1} \exp(2\pi i(k-j)n/N) = N\delta_{k\,j} \tag{8}$$

This means that the computation of the integrals (7) by means of the trapeze method is exact (within the round-off errors). In the theory of signal, the Gauss-Lobatto points correspond to the Shanonn sampling, and $N/2-1$ is related to the Shanonn frequency.

of x) is performed only for practical convenience, for example to visualize the solution at a given time. Consequently, the configuration space plays a secondary role.

The second way to proceed *(pseudo-spectral method)* consists in computing the derivative of u in the Fourier space, to come back in the configuration space by an inverse Fourier transform, to multiply $\partial u/\partial x$ by u in the configuration space and to come back again in the Fourier space. With pseudo-spectral method, the Fourier and configuration spaces behave equally. Pseudo-spectral method is generally used in spite of the apparent athletic work of dancing from one space to the other. The reason is that performing a convolution requires a number of operations proportional to N^2. On the contrary, thanks to the fast [2] Fourier algorithm, the number of operations needed by pseudo-spectral method is proportional to $N \log N$. Moreover the pure spectral method can not handle easily non-linearities more general than the quadratic one present in (3). In all this paper, we shall use (incorrectly) for shortness the term of *spectral method* instead of the more appropriate *pseudo-spectral method*.

The above example contains all the philosophy of SM. A PDE, or more generally a system of PDEs, is transformed in an equivalent system of ordinary differential equations. The set of trigonometric functions used for the expansion, has been chosen because it fulfils automatically the boundary conditions and because it exists a fast transform algorithm. The space derivatives are computed in the coefficients space and the computation uses the value of the function on *all* collocation points. Quadratic terms are computed by coming back to the configuration space. The most important consequence is that if the solution is C^∞ then the $\mathcal{L}^2$ error between the numerical solution and the analytical one scales as $\exp(-N)$ and as $N^{-(p+1)}$ for a solution C^p [3]. An error that scales as $\exp(-N)$ is called *evanescent*.

Finally the computation of the required quantities is performed in one of the two spaces, namely the configuration space or its dual (Fourier space), in order to save computation time and to obtain high accuracy.

[2] A 1-D numerical algorithm is called *fast* if the number of arithmetic operations scales with the number of the degrees of freedom N no faster than $N \log N$. Fast Fourier Transform (FFT) and Fast Chebyshev transform algorithms (FCT) are *fast* algorithms.

[3] Following the terminology of the functional analysis, the error $\mathcal{L}^p$ of some numerical solution $u_{\rm num}(x,t)$ is defined by

$$\left(\int_{-1}^{1} [u_{\rm num}(x,t) - u_{\rm ex}(x,t)]^p \, dx \right)^{1/p} \tag{9}$$

where $u_{\rm ex}(x,t)$ is the exact solution.

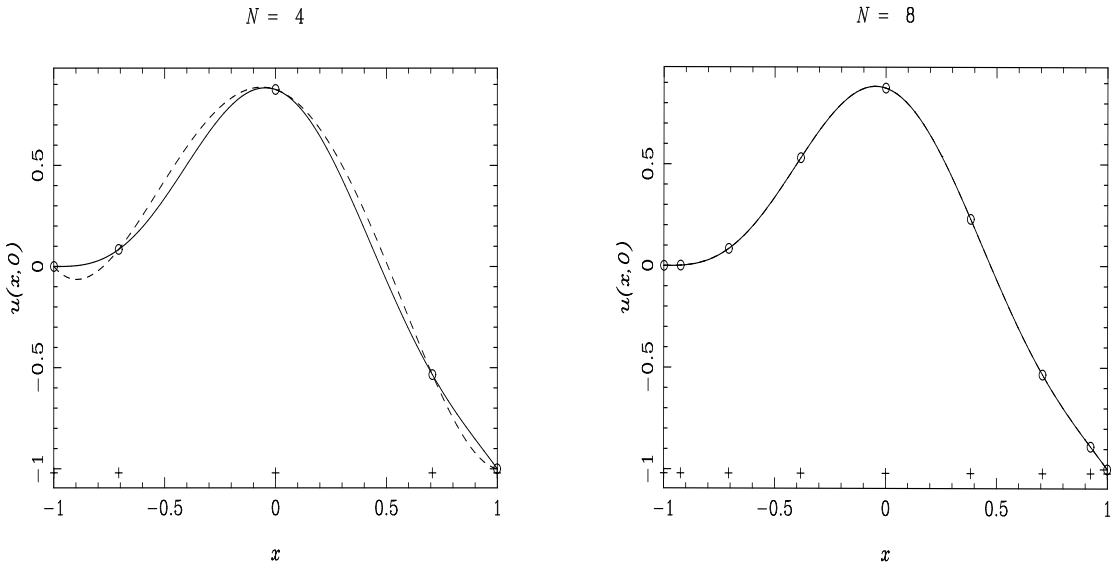

Fig. 1. Graph of the function $u(x) = \cos^3(\pi\, x/2) - (x+1)^3/8$ (solid line) and its Chebyshev interpolant (dashed line) for $N = 5$ (left) and $N = 9$ (right). For $N = 9$, the two curves cannot be distinguished graphically. The circles denote the values at the collocation points x_n. Note that spurious oscillations between the collocation points are not present.

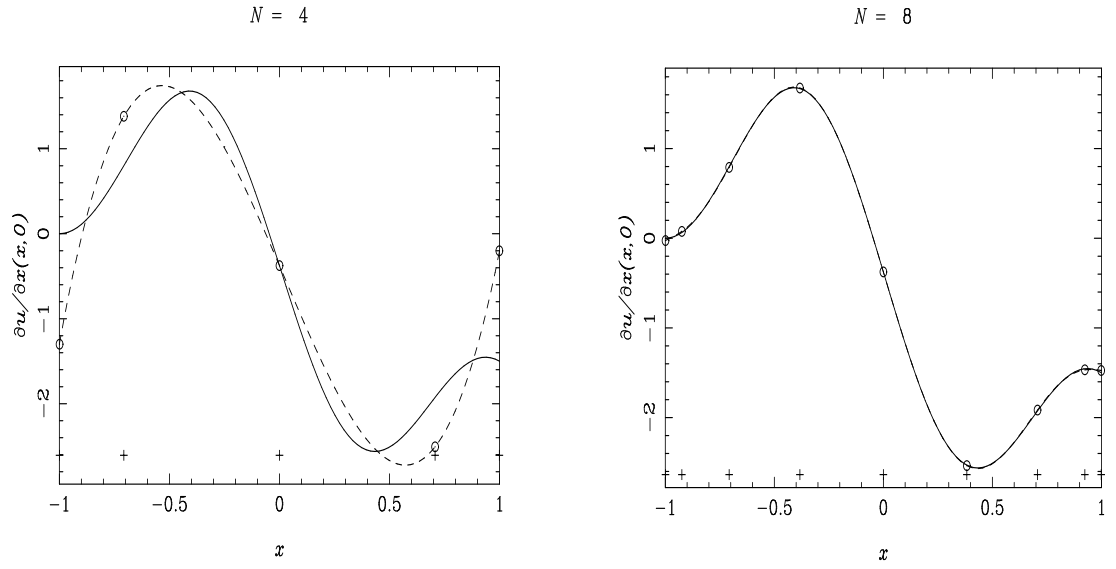

Fig. 2. Graph of the derivative of the function represented in Fig. 1 Eq. (12) (solid line) and its Chebyshev approximation (dashed line), for $N = 5$ (left) and $N = 9$ (right). The circles denote the values at the collocation points x_n.

2.2 More general expansions

If the initial conditions or the boundary conditions are not periodic, Fourier expansion is no more adapted to treat the problem because of the presence of a Gibbs phenomenon at the boundaries of the interval [4]. A new base of functions must be used. Expansions in Legendre or Chebyshev polynomials are the most common ones. The reader will find in [21] and [18] a discussion on the advantage and drawbacks of the different expansions. Legendre polynomials are often used for theoretical work [36]. The main advantage of Chebyshev polynomials is that there exists a fast algorithm to perform Chebyshev expansion (its C.P.U. time is just a little bit longer than the corresponding Fourier transform time). For this reason, Chebyshev expansion is widely used in this paper.

Chebyshev polynomials $T_n(x)$ are defined as the family of polynomials which obeys to the the following orthogonality relations:

$$\frac{(1+\delta_{n\,0})}{\pi}\int_{-1}^{1}\frac{T_n(x)T_m(x)}{\sqrt{1-x^2}}dx=\delta_{n\,m}\ , \tag{10}$$

where $\delta_{n\,m}$ is the Kronecker symbol. By introducing the new variable $\theta = \arccos(x)$ $(0 \leq \theta \leq \pi)$, the Chebyshev polynomials read

$$T_n(x(\theta)) = \cos(n\theta)\ . \tag{11}$$

The associated Gauss-Lobatto points x_j are uniformly spaced with respect to the variable θ: $x_j = \cos(\pi(j-1)/(N-1))$, $\quad 0 \leq j \leq N-1$ where N is the number of degrees of freedom. It easy to see that the collocation points are more dense close to the boundaries of the interval $[-1,+1]$. Thanks to the relation (11), Chebyshev polynomials have close links to the trigonometric functions used in the Fourier expansion.

The following example illustrates the accuracy of SM. Let us consider the function

$$u(x) = \cos^3\left(\frac{\pi}{2}x\right) - \frac{1}{8}(x+1)^3 \qquad x \in [-1,1]\ . \tag{12}$$

[4] The Gibbs phenomenon occurs when an expansion, for example the Fourier expansion, of a discontinuous function is performed. In this case the $\mathcal{L}^2$ error scales with the degrees of freedom N as $1/N$. On the contrary the pointwise error $\mathcal{L}^\infty$ tends to a finite value when $N \to \infty$ (see e.g. ref. [21])

NDF	error on $\frac{du}{dx}$		error on $\frac{d^2u}{dx^2}$	
	SM	FDM	SM	FDM
5	5.8E-01	8.2E-02	2.1E+00	3.7E+00
7	1.2E-01	5.5E-01	3.4E-01	2.2E+00
9	1.2E-02	5.1E-01	5.8E-02	1.4E+00
13	2.8E-05	2.6E-01	3.6E-04	6.8E-01
21	4.2E-12	1.0E-01	1.6E-10	2.6E-01
33	1.5E-13	4.0E-02	2.9E-11	1.0E-01
65	3.2E-13	1.0E-02	5.6E-10	2.6E-02
129	2.5E-11	2.5E-03	1.4E-07	6.4E-03
513	1.4E-09	1.6E-04	8.6E-05	4.0E-04
1025	1.6E-08	4.0E-05	5.3E-03	1.0E-04

Table 1
Comparison between a Chebyshev spectral method (SM) and a second-order finite difference method (FDM) in the computation of the first and second derivatives of the function $u(x) = \cos^3\left(\frac{\pi}{2}x\right) - (x+1)^3/8$. The error is defined as the highest discrepancy with the exact value at the grid points. 16 digits are used in the numerical computation. Note that to obtain an accuracy on d^2u/dx^2 of the order 10^{-4}, 13 points are sufficient for the SM, whereas the FDM requires about 500. Note also that for NDF ≥ 129, the round-off errors make the SM less efficient.

Note that $u(x)$ is not a polynomial, so that its expansion over the Chebyshev polynomials a priori requires an infinite number of coefficients. The term $(x+1)^3$ has been added to the cosine term in order not to have a periodic function. The function $u(x)$ is represented in Fig. 1, as well as its Chebyshev interpolant $\sum_{n=0}^{N-1} \hat{u}_n T_n(x)$ for $N = 5$ and $N = 9$. Note that for a number as small as $N = 9$, the Chebyshev expansion cannot be graphically distinguished from u. The derivative of $u(x)$ is numerically computed by means of the method described in Sect. 3.1 and is compared with its analytical value in Fig. 2.

The comparison with a second-order finite difference method is performed in Table 1 for the computation of the first and second derivatives of u. Note that for $N = 33$, the SM reaches a relative accuracy of 1.5×10^{-13} and 3×10^{-11} in the computation of du/dx and d^2u/dx^2 respectively.

3 Algebraic properties and spectral representation of some elementary operators

We will discuss in this section some properties and implementation of elementary linear differential operators when using Chebyshev polynomial expansions.

3.1 First and second order derivatives.

The expansion coefficient b_i of df/dx are given by $b_i = D_{ij}a_j$ where a_i are the coefficients of f and, by definition of d/dx,

$$D_{ij} = (2 - \delta_0^i) \int_{-1}^{1} T_i(x) T'_j(x) (1 - x^2)^{-1/2} dx \ . \tag{13}$$

The matrix D_{ij} is computed from the relation

$$T'_{n+1}(x) = 2(n+1)\, T_n(x) + \frac{n+1}{n-1} T'_{n-1}(x) \ , \tag{14}$$

which can be derived easily from Eq. (11). For a NDF = 7, the result is:

$$D_{ij} = \begin{bmatrix} 0 & 1 & 0 & 3 & 0 & 5 & 0 \\ 0 & 0 & 4 & 0 & 8 & 0 & 12 \\ 0 & 0 & 0 & 6 & 0 & 10 & 0 \\ 0 & 0 & 0 & 0 & 8 & 0 & 12 \\ 0 & 0 & 0 & 0 & 0 & 10 & 0 \\ 0 & 0 & 0 & 0 & 0 & 0 & 12 \\ 0 & 0 & 0 & 0 & 0 & 0 & 0 \end{bmatrix} . \tag{15}$$

The disposition of the non vanishing elements of D_{ij} is due to the property of the operator d/dx which transforms the parity of the functions at which is applied. The main diagonal and the last line of D_{ij} vanish because the operator d/dx transforms a polynomial of degree n into a polynomial of degree $n-1$. These two important properties will be used below.

The representation of the operator d^2/dx^2 can be obtained straightforwardly by taking the square of the matrix (15). For a NDF = 7, it reads

$$D^2_{ij} = \begin{bmatrix} 0 & 0 & 4 & 0 & 32 & 0 & 108 \\ 0 & 0 & 0 & 24 & 0 & 120 & 0 \\ 0 & 0 & 0 & 0 & 48 & 0 & 192 \\ 0 & 0 & 0 & 0 & 0 & 80 & 0 \\ 0 & 0 & 0 & 0 & 0 & 0 & 120 \\ 0 & 0 & 0 & 0 & 0 & 0 & 0 \\ 0 & 0 & 0 & 0 & 0 & 0 & 0 \end{bmatrix} \tag{16}$$

The disposition of the zeros is different, because the operator d^2/dx^2 preserves the parity. The last two lines of the matrix vanish because this operator decreases the degree of a polynomial by two units. Other operators that preserve the number of coefficients are

$$x\frac{d}{dx}\,, \quad (ax + bx^2)\frac{d^2}{dx^2} \tag{17}$$

These operators play an important role in solving PDEs.

The computation of the derivative of a function f obtained by a matrix multiplication needs a number of multiplication $\propto N^2$. Actually, the particular structure of the matrix (15) suggests not to perform the full matrix multiplication but instead to use the recursion formula

$$\hat{f'}_n = 2(n+1)\hat{f}_{n+1} + \hat{f'}_{n+2} \qquad n \leq N-2\ , \tag{18}$$

A similar recursion law exists for the operator d^2/dx^2. In a such a way the number of operations becomes $\propto N$. Hereafter we shall call *fast* an algorithm requiring a number of elementary operations $\propto N$ or $\propto N \ln N$ where N is the NDF.

3.2 Primitive of a function

A primitive $F(x)$ of a function $f(x)$ can be obtained by inversion of the operator d/dx, i.e. by solving the algebraic system of N equations

$$\sum_{n=0}^{N-1} D_{mn} b_n = a_m\ , \tag{19}$$

where b_m are the expansion coefficients of F. The determinant of D_{nm} vanishes because the primitive of a function is defined within some additive constant.

We can add an algebraic condition, for instance $F(-1) = 0$, in order to eliminate this degeneracy. One (certainly not unique !) way to proceed is to seek for a primitive that has some property in the coefficient space, for instance that its first coefficient b_0 vanishes. That is equivalent to find a particular solution F_p of the differential equation $dF/dx = f$. Once this solution is found, we can add to it a homogeneous function F_h in such a way that the final solution $F = F_p + F_h$ fulfils the required conditions. In this example F_h is constant. If we look for a particular solution having $b_0 = 0$, the new system is

$$\begin{bmatrix} 1 & 0 & 0 & 0 & 0 & 0 & 0 \\ 0 & 2 & 0 & 0 & 0 & 0 & 0 \\ 0 & 0 & 4 & 0 & 0 & 0 & 0 \\ 0 & 0 & 0 & 6 & 0 & 0 & 0 \\ 0 & 0 & 0 & 0 & 8 & 0 & 0 \\ 0 & 0 & 0 & 0 & 0 & 10 & 0 \\ 0 & 0 & 0 & 0 & 0 & 0 & 12 \end{bmatrix} \begin{bmatrix} b_0 \\ b_1 \\ b_2 \\ b_3 \\ b_4 \\ b_5 \\ b_6 \end{bmatrix} = \begin{bmatrix} 0 \\ \tilde{a_0} \\ \tilde{a_1} \\ \tilde{a_2} \\ \tilde{a_3} \\ \tilde{a_4} \\ \tilde{a_5} \end{bmatrix} \tag{20}$$

where $\tilde{a_j}$ is the new RHS vector corresponding to the linear combination

$$\tilde{D}_{mn} = D_{mn} - \frac{1}{1+\delta_m^0} D_{m+2,n} \qquad 0 \le m \le N-4 \ , \tag{21}$$

which transforms the matrix D_{mn} into a diagonal one. It follows that the computation of the primitive of a function can be performed with a fast algorithm. This technique is quite general and is similar to that used when treating more complicated problems (cf. Sect. 4.5).

3.3 Reduction to band matrices of more general operators

The matrix representation D^2_{mn} of the operator d^2/dx^2 can also be transformed to a band matrix with some simple linear combination of the lines. Applying first the linear combination

$$\tilde{D}^2_{mn} = \frac{(1+\delta_0^m) D^2_{mn} - D^2_{m+2,n}}{m+1} \qquad 0 \le m \le N-3 \tag{22}$$

followed by

$$\bar{D}^2_{mn} = \tilde{D}^2_{mn} - \tilde{D}^2_{m+2\,n} \qquad 0 \le m \le N-5 \tag{23}$$

transforms the matrix into

$$\bar{D}^2_{nm} = \begin{bmatrix} 0 & 0 & 8 & 0 & 0 & 0 & 0 \\ 0 & 0 & 0 & 12 & 0 & 0 & 0 \\ 0 & 0 & 0 & 0 & 16 & 0 & 0 \\ 0 & 0 & 0 & 0 & 0 & 20 & 0 \\ 0 & 0 & 0 & 0 & 0 & 0 & 24 \\ 0 & 0 & 0 & 0 & 0 & 0 & 0 \\ 0 & 0 & 0 & 0 & 0 & 0 & 0 \end{bmatrix} \tag{24}$$

More generally, the matrix representation of the differential operator

$$\mathbf{L} = \mathbf{I} + (a_0 + a_1 x)\frac{d}{dx} + (b_0 + b_1 x + b_2 x^2)\frac{d^2}{dx^2} \ , \tag{25}$$

where $\mathbf{I}$ is the identity and a_0, a_1, b_0, b_1 and b_2 are numerical constants, can be transformed to a penta-diagonal matrix via the linear combinations (22) and (23). Therefore there exists a fast algorithm to inverse the above operator. Note that the operator $\mathbf{I}$ is responsible for the five diagonals of the matrix.

Finally, the multiplication and division of a function by $X = a+bx$ can be performed in the coefficient space. The matrix representation of this operation is a bi-diagonal matrix X_{ij}. Therefore multiplication and division are performed with a fast algorithm. The advantages in operating in this way are the following ones. Firstly, it is easier to handle the division by X when X vanishes for a given value of x. Moreover, the roundoff error is less important than when performing the multiplication in the configuration space. Secondly, computing quantities like $(x+1)^l$, (l integer ≥ 1) in the configuration space introduces high frequency terms. In fact, for large values of l, the function $(1+x)^l$ is numerically zero and therefore not continuous near $x = -1$. Such functions play an important role in spherical coordinates, because they are the radial part of the spherical harmonics of order l. Thirdly, it avoids to come back to the configuration space to perform the multiplication by x when the function is known in the coefficient space.

4 Solution of elementary P.D.E. in Cartesian coordinates

4.1 Temporal scheme

Consider the 1-D second order hyperbolic PDE (heat equation with advection)

$$\frac{\partial \Theta}{\partial t} + v(x)\frac{\partial \Theta}{\partial x} - \mu(x)\frac{\partial^2 \Theta}{\partial x^2} = S(x,t) \quad x \in [-1,+1],\ t \geq 0 \ . \tag{26}$$

If $\mu(x) = 0$ and $v(x) = v_0 = \text{const}$, the general solution is $\Theta(x,t) = f(x - v_0 t)$ i.e. a wave propagating from the left to the right if $v_0 > 0$ and from the right to the left in the opposite case. The time evolution of Θ can be obtained by computing the time derivative with a finite difference method: t is discretized at given uniformly spaced instants t_j, $t_{j+1} = t_j + \Delta t$ and a second order scheme (for example an explicit Crank-Nicolson scheme) approximates, Eq. (26) by

$$\Theta^{j+1} - \Theta^j = -\frac{\Delta t}{2}\left(v\frac{\partial \Theta}{\partial x}^{j+1} + v\frac{\partial \Theta^j}{\partial x} + S^{j+1/2}\right) , \tag{27}$$

where $\partial\Theta^{j+1}/\partial x$ at the RHS is computed by extrapolating its values from the past. This scheme is highly unstable, no matter the choice of the time-step Δt. This instability is due to the absence of boundary conditions. The value of Θ at $x = -1$ if $v_0 > 0$ or at $x = 1$ in the opposite case, must be given. In other words, we have to define what goes into the interval $[-1, +1]$.

Before to explain which boundary condition makes the problem well posed (in the sense given by Hadamard, see e.g. [50] p. 62) and how it can be implemented, it is worth to discuss the Courant conditions that garanties the numerical stability.

In the case of Chebyshev polynomial expansion, the numerical stability is achieved if $\Delta t \propto 1/N^2$. This condition (Courant condition) is much more severe than in the case of finite difference method with uniform grid for which $\Delta t \propto 1/N$. The situation is much worse if a spatial second order operator is present ($\mu(x) \neq 0$). In this case Δt must decrease as $1/N^4$. These severe Courant condition is due to the fact that the density of the Chebyshev collocation points behave like $1/N^2$ near the boundaries $x = -1$ and $x = +1$ (see e.g. Fig. 1 or Fig. 3). However, if the coefficients of the space derivatives vanish at the boundaries, the Courant condition becomes $\Delta t \propto 1/N$ in the case of a first order spatial differential operator and $\Delta t \propto 1/N^2$ in the case of a second order spatial differential operator. Note that the dense sampling at the boundaries can also be an advantage: it is well suited to resolve boundary layers if they are present in the solution. We shall give an example below (Sect. 5.2).

Implicit (or semi-implicit) schemes allow to overcome this difficulty. Implicitation of the Crank-Nicolson scheme (27) can be obtained by inverting the operator $Id + \Delta t\partial/\partial x$. The generalization to the case $\mu(x) = \mu_0 = const. \neq 0$ is straightforward. With an implicit scheme the absolute convergence (for any value of Δt) is obtained.

The leapfrog scheme, which is very widely used with Fourier expansion, turns out to be unstable with Chebyshev expansion. The reader will find an exhaustive discussion on this subject in [21] pp. 103-115. In the present arti-

cle, we shall use systematically the Crank-Nicolson scheme. Its accuracy behaves like Δt^3 per time-step when all the quantities are computed at the time $t^{j+1/2} = t^j + \Delta t/2$.

In a more general case, when the coefficients of the spatial derivatives depend on x, the implicitation consists to invert an operator of the kind $\mathcal{O} = Id + b(x,t)D$ where Id and D are respectively the identity and a differential operator and where $b(x,t)$ is some function. The matrix representation of operator $\mathcal{O}$ is in general a full matrix which cannot be reduced to a band matrix by means of simple operations. Consequently, the inversion of $\mathcal{O}$ operator requires a number of operations $\propto N^3$. In order to save CPU time and to build a fast algorithm, the following *semi-implicit* method is highly recommended.

Consider for simplicity Eq. (26) with $v(x) = 0$. If the Crank-Nicolson scheme is used, the corresponding PDE reads

$$\Theta^{j+1} - \frac{1}{2}\Delta t\, \mu(x)\frac{\partial^2 \Theta^{j+1}}{\partial x^2} = \Theta^j + \frac{1}{2}\Delta t\, \mu(x)\frac{\partial^2 \Theta^j}{\partial x^2} + S(x)^{j+1/2}\ . \qquad (28)$$

The above time discretization can be reformulated in the equivalent form

$$\Theta^{j+1} - \frac{1}{2}\Delta t\, \mu^{max}\frac{\partial^2 \Theta^{j+1}}{\partial x^2} = \Theta^j + \frac{1}{2}\Delta t\, \mu(x)\frac{\partial^2 \Theta^j}{\partial x^2} - \frac{1}{2}\Delta t(\mu^{max} - \mu(x))\frac{\partial^2 \Theta^{j+1}}{\partial x^2} + S(x)^{j+1/2}\ , \qquad (29)$$

where μ^{max} is the maximum value of $\mu(x)$ on the interval $[-1,+1]$. The RHS of Eq. (29) becomes the source of the new equation. The term $(\mu^{max} - \mu(x))\partial^2\Theta^{j+1}/\partial x^2$ is computed by means of a second order extrapolation from its value at the items t^{j-2}, t^{j-1}, t^j. In this way, we reduce the problem to the case of constant coefficients.

It is obvious that the new temporal scheme is of second order too. However, its precision depends on how close $\mu(x)$ is to μ^{max}. Moreover, this method cannot be applied straightforwardly to the case where $\mu(x)$ vanishes at the boundary of the interval.

To improve the method, we can introduce a polynomial $P_2(x) = a_0 + a_1 x + a_2 x^2$ instead of μ^{max} which behaves as $\mu(x)$ at the boundaries and such that $P_2(x) - \mu(x) \geq 0$. As mentioned in Sect. 3.3, the matrix representation of the operator $Id + P_2(x)\partial^2/\partial x^2$ can be reduced to a penta-diagonal matrix by means of the linear combination (22)-(23). The generalization to the case $v(x) \neq 0$ is obvious.

Implicit or semi-implicit temporal scheme in multi-dimensional problems can be easily implemented with the Alternating Direction Method (cf. [51]). We have tested this method for 2-D problems and did not found any difficulty. We conjecture that this method can be used for 3-D problems too.

4.2 Boundary conditions and well posed problems

Because of its generality, we will use equation (26) to discuss in detail the numerical problems tied to boundary conditions and its solution.

The problem is well posed in the following cases.

- If $\mu(x) = 0$, the equation reduces to a first order PDE. In this case, if $v(x) \neq 0$ for $x \in [-1, +1]$ then one BC at $x = -1$ ($v(x) > 0$) or at $x = +1$ ($v(x) < 0$) must be imposed.

- If $\mu(x) = 0$ and $v(x) \geq 0$ for $x \in [-1, +1]$ and $v(-1) = 0$ then no BC can be imposed. The same holds if $v(x) \leq 0$ for $x \in [-1, +1]$ and $v(+1) = 0$.

- If $\mu(-1) = \mu(+1) = v(x) = 0$ but $\mu(x) > 0$ for $x \in]-1, +1[$, the rules given for the first order PDE hold.

- If $\mu(x)$ and $v(x)$ vanish on the boundaries, only one BC is required (as in the previous case).

- If $\mu(x) > 0$ everywhere, two BC are required.

For a second order PDE, boundary conditions are quite general and can have the form

$$\alpha(t)\frac{\partial \Theta}{\partial x} + \beta(t)\Theta = \gamma(t) \ , \tag{30}$$

but other non local BC (dual BC) can be chosen (see below). An example of a not well posed problem is to impose two BC (the value of Θ and its derivative) at one boundary of the interval.

4.3 Boundary layer and dual boundary conditions

Consider Eq. (26) with μ and v constant: $\mu(x) = \mu_0$, $v(x) = v_0 > 0$. If $\mu_0 \to 0$, the equation degenerates in a first order equation. We can not impose two BC in the case of a first order equation. Physically, when $\mu_0 \to 0$, a

boundary layer is formed at $x = +1$ and the numerical algorithm has been able to describe the strong variation of the solution near the boundary. We can form an adimensional parameter N_p (the *Péclet number*) which characterizes the thickness of the layer : $N_p = v_0 L/\mu_0$ where L is the typical dimension of the system. The thickness D_l of the layer is $D_l = L/N_p$. In this example, $L = 2$ and $N_p = 2v_0/\mu_0$. Thanks to the accumulation of collocation points at the boundary, Chebyshev expansion is well suited to treat this problem. The layer is well resolved and the maximum value of N_p which garanties numerical stability scales as $N^{7/4}$. For instance with $N = 33$ collocation points N_p can be as high as 200 (see e.g. [21] p. 140).

In physical applications, it can happen that a fine resolution of the boundary layer is not required. The natural question arises how modify the BC in such a way that the new solution differs appreciably from the exact one only in the layer. It is clear that the boundary layer is created by the BC that not would exist in the case $\mu_0 = 0$. Unfortunately, numerical instabilities appear if only one BC is imposed when $\mu_0 \neq 0$. To overcome this difficulty, we need to find a criterium which leads to a value of Θ at the boundary where the layer forms ($x = +1$) such that the numerical scheme is stable if $\mu_0 = 0$ too. In other words, we need a redundant BC.

Such a BC is more general than the usual one. We will call it a "non local" boundary condition because this condition is imposed in the coefficients space. There is a wide class of criteria to find a magic value for $\Theta(+1)$. One criterium consists in finding $\Theta(+1)$ such that, at each time step, $\Theta(x)$ is as smooth as possible. For instance, one can minimize the norm of $\partial^2\Theta(x)/\partial x^2$ i.e.

$$\int_{-1}^{1} \left(\frac{\partial^2 \Theta(x)}{\partial x^2} \right)^2 dx \ , \tag{31}$$

Another method consists to cancel the last coefficient of the expansion of Θ or to minimize the sum of the square of the last J coefficients. All these exotic BC garanties the stability of the numerical scheme for any value of $\mu_0 \geq 0$ and gives very similar results. Note that the last two criteria introduce an evanescent error when $\mu(x) = 0$.

An heuristic justification of this procedure can be easily understood by noting that the Péclet number parametrizes the antagonism between the advection term $v_0 > 0$, which carries the information from the left to the right, and the diffusion term μ_0 which diffuses back the information. For high Péclet numbers, the diffusion term influences only the boundary layer. Therefore, the solution outside of the layer is almost not influenced by the BC.

The above exotic BC are useful in other physical situations. Consider a region

R of the interior of a star. Let us suppose that we are interested in phenomena described by a PDE of the kind of Eq. (26) only in this region. We need to know which BC to impose at the boundary of R. This BC cannot be known without solving the equation in *all* the star. We know only that the solution is smooth in the interior of the star. Therefore, we can impose a value of the solution which makes the solution as smooth as possible. Roughly speaking, the underlying philosophy is to introduce the minimum of information when the problem is not completely determined. The reader will recognize the same philosophy which underlies the maximum entropy criterium used in the theory of signal.

4.4 Implementation of the boundary conditions

There are various ways to implement the BC within spectral methods. We present here three different methods.

4.4.1 Galerkin method

The *Galerkin method* consists in choosing the set of functions used for the expansion a set of function satisfying the required BC. The example showed in Sect. 2.1 solves a PDE with periodical BC by means of Fourier expansion. The Galerkin method will be widely used to handle regularity conditions (e.g. with spherical coordinates where coordinate singularities appear). It is sometimes easy to find a set of functions satisfying the desired BC by taking a linear combination of Chebyshev polynomials. For instance, if the solution of the PDE must vanish at $x = -1$, one can expand the quantities onto the new basis of function Φ_n :

$$\Phi_n(x) = T_n(x) + T_{n+1}(x) \ . \tag{32}$$

Note that the matrix of the corresponding linear algebraic system of equations can be reduced to a band matrix via the linear combinations (22),(23). However, the number of diagonal is larger: the 5 diagonals for Eq.(26) become 7 when the above Galerkin basis is used.

4.4.2 Lanczos method

The *Lanczos method* [33] consists to replace the source $S_n^{j+1/2}$ (in the coefficient space) of Eq. (26) by

$$\tilde{S}_n = S_n^{j+1/2} + b_1 \delta_{N-1,n} + b_2 \delta_{N,n} \ , \tag{33}$$

where $\delta_{n,m}$ is the Kronecker symbol and to compute, at each time step, the coefficients b_1 and b_2 in such a way that BC are fulfilled (cf. Sect. 4.5).

4.4.3 Dual Lanczos method

A *dual Lanczos method*[5] consists to add in the configuration space two Dirac's functions to the solution. The coefficients of these δ function are computed in order to satisfy the BC. The source $S^{j+1/2}(x_k)$ is replaced by

$$\tilde{S}(x_k) = S(x_k)^{j+1/2} + b_1\delta(x_k, -1) + b_2\delta(x_k, 1) \ . \tag{34}$$

These three methods can be used either with explicit or implicit temporal scheme. From the numerical point of view, the implicit scheme must be treated carefully, especially for second order equations when the time step is large.

4.5 Details about the boundary condition implementation

Let us consider the heat equation (26) with $v(x) = 0$ and $\mu(x) = 1$ and let us suppose that the time discretization is performed according to a first order fully implicit time scheme. For $\Delta t = 0.1$, the system to be solved is then (cf. Eq. (16)):

$$\begin{bmatrix} 1 & 0 & -.4 & 0 & -3.2 & 0 & -10.8 \\ 0 & 1 & 0 & -2.4 & 0 & -12 & 0 \\ 0 & 0 & 1 & 0 & -4.8 & 0 & -19.2 \\ 0 & 0 & 0 & 1 & 0 & -8 & 0 \\ 0 & 0 & 0 & 0 & 1 & 0 & -12 \\ 0 & 0 & 0 & 0 & 0 & 1 & 0 \\ 0 & 0 & 0 & 0 & 0 & 0 & 1 \end{bmatrix} \begin{bmatrix} \Theta_0 \\ \Theta_1 \\ \Theta_2 \\ \Theta_3 \\ \Theta_4 \\ \Theta_5 \\ \Theta_6 \end{bmatrix} = \begin{bmatrix} \tilde{S}_0 \\ \tilde{S}_1 \\ \tilde{S}_2 \\ \tilde{S}_3 \\ \tilde{S}_4 \\ \tilde{S}_5 \\ \tilde{S}_6 \end{bmatrix} \ , \tag{35}$$

where the R.H.S. of the system, $\tilde{S}_n$, is the Lanczos modified source defined by Eq. (33) or by Eq. (34) depending on the choice of the BC treatment method. The simplest way to find the value of the coefficients b_1 and b_2 is to solve first the system having as source the vector S_n only ($b_1 = b_2 = 0$). In this way one particular solution $\Theta_n^{\rm par}$ of the system is found. The second step consists in finding two homogeneous solutions $\Theta_n^{\rm h1}$ and $\Theta_n^{\rm h2}$ by solving twice the system (35) with the source $\delta_{N-1,n}$ and $\delta_{N-2,n}$ (for the Lanczos method) and finally

[5] In the book by Gottlieb & Orszag [21], this method is called *collocation approximation* (page 14 of [21]). We prefer the term *dual Lanczos method* for obvious reasons.

by computing b_1 and b_2 in order to fulfil the required BC. The same procedure holds for the dual Lanczos method. We recall that the Chebyshev coefficients of the Dirac functions at the interval boundaries, namely $\delta(x+1)$ and $\delta(x-1)$, are respectively $\hat{\delta}_n = (-1)^{n-1}$ and $\hat{\delta}_n = 1$. Of course, as already said, the matrix of the above system can be reduced with simple linear combinations to a penta-diagonal matrix and consequently finding solutions of a banded system having 3 different R.H.S. is a very little time consuming. The homogeneous solution can be used to satisfy the dual BC by imposing, for example, that the last coefficient of the solution vanishes. By looking at the matrix of the system (35), it appears that the extra-diagonal coefficients for $\Delta t = .1$ are much larger than the coefficients of the main diagonal. It follows that each solution of the system depends strongly on the value of the highest order coefficients of the source (this is a consequence of the fact that the problem is not well posed without BC). Moreover, small values of the highest order coefficients lead to very large solutions. When the linear combination of the 3 solutions required to fulfil the correct BC is performed compensations occur to give the correct solution. These compensations are source of important round-off errors. In practice, $\Delta t \propto 1/N^3$ is a necessary condition to have high precision results. Another procedure works in the opposite case (Δt high) and is easy to implement for the Lanczos method. It is the following one: look for a solution of the first equation having some condition in the coefficient space, for example having the two first coefficients vanishing. This can be obtained easily by replacing the system (35) by

$$\begin{bmatrix} 1 & 0 & 0 & 0 & 0 & 0 & 0 \\ 0 & 1 & 0 & 0 & 0 & 0 & 0 \\ 1 & 0 & -.4 & 0 & -3.2 & 0 & -10.8 \\ 0 & 1 & 0 & -2.4 & 0 & -12 & 0 \\ 0 & 0 & 1 & 0 & -4.8 & 0 & -19.2 \\ 0 & 0 & 0 & 1 & 0 & -8 & 0 \\ 0 & 0 & 0 & 0 & 1 & 0 & -12 \end{bmatrix} \begin{bmatrix} \Theta_0 \\ \Theta_1 \\ \Theta_2 \\ \Theta_3 \\ \Theta_4 \\ \Theta_5 \\ \Theta_6 \end{bmatrix} = \begin{bmatrix} 0 \\ 0 \\ S_0 \\ S_1 \\ S_2 \\ S_3 \\ S_4 \end{bmatrix} . \quad (36)$$

In this way we have found a particular solution having the two first coefficients vanishing. Find then two other homogeneous solutions having as source $\delta_{1,n}$ and $\delta_{2,n}$ and make a linear combination in order to fulfil the BC. It is obvious that the solution obtained in this way is the same than that obtained by solving the original system (35): both solutions satisfy indeed the first $N-2$ equations and the BC; the unicity theorem garanties that the two solutions are identical.

The matrix of the new system has the coefficients of main diagonal which increase when N increases and the solution is computed with high accuracy for $\Delta t > 1/N^4$. In fact, in the opposite case, the determinant of the new matrix vanishes for $\Delta t = 0$ and the round-off errors become important for too

small values of Δt. Therefore the solution method depends on the value of N and Δt. We recommend the Lanczos method for large values of Δt and the dual method in the opposite case. For first order equations, or for the advective diffusive equation with high Péclet numbers, the dual Lanczos method is more convenient.

4.6 Artificial spectral diffusivity

In classical hydrodynamics with finite difference methods, artificial viscosity or diffusivity is often used in order to avoid singularities in the numerical solutions and/or to stabilize the numerical scheme.

Within Fourier expansion, a high order operator is added to the RHS of the PDE in order to obtain a smoother solution. In the Fourier space, this artificial diffusivity is of the kind $\propto k^{2L}$ [2] (L integer number) where k is the spatial frequency. For $L = 1$, this term represents the ordinary diffusivity. For $L \to \infty$, its tends to the *evanescent viscosity* introduced by Maday et al. [36]. Within Chebyshev expansion, spectral viscosity can be implemented via a power of the degenerated operator $\mathcal{V} = \sqrt{1-x^2}d/dx\left[\sqrt{1-x^2}d/dx\right]$ [37]. This is an extension to Chebyshev SM of the technique developed in [2] for Fourier SM. Its matrix representation is a diagonal matrix: $V_{nm} = -n^2\delta_{nm}$. Analogous *linear* artificial viscosity methods were used in numerical magneto-hydrodynamics for handling sharp gradients induced by non-linearities [29,52,35]. Non-linear artificial viscosity (*hyperviscosity*) has been introduced in [48] and applied to MHD problems [47].

5 Examples of time evolution

5.1 Advection equation

In view to compare the different approximations we start with the advection equation (26) with $\mu(x) = 0$ and $v(x) = 1$. We choose $\Theta(x, 0) = 0$ and $\Theta(-1, t) = \sin(4\pi t)^2$. The analytical solution of this PDE is $\Theta_{\rm ana}(x, t) = \sin(4\pi(t-x))^2$ and will be used to compute the numerical error. Spectral methods are not well suited to solve hyperbolic equations; this example is worth to show why. Figure 3 shows the solution computed by means of a Chebyshev expansion and an implicit Crank-Nicolson scheme, with the Lanczos approximation (Sect. 4.4). The corresponding numerical error is shown in Fig. 4. The solution is $\mathcal{C}^1$. Therefore the errors decreases as $1/N^2$ and Gibbs phenomenon is heavily present. The solution becomes C^∞ only when the front of the wave

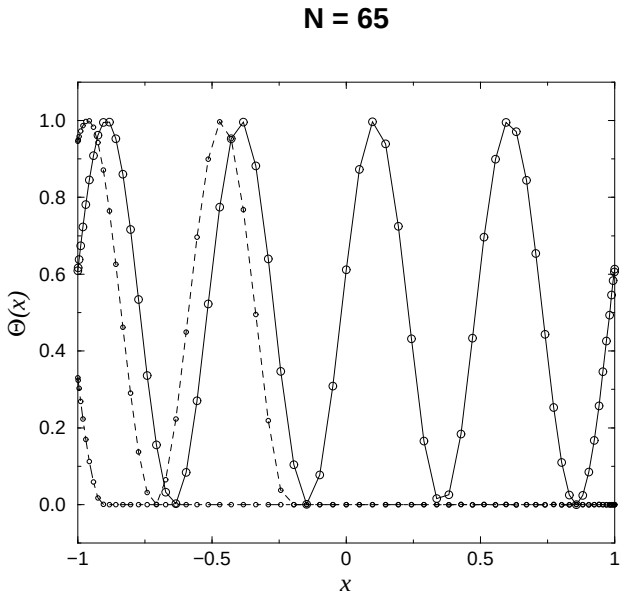

Fig. 3. Profiles at different time steps (long dashed, short dashed and solid line successively) of the solution of the advection equation (Eq. (26) with $v(x) = 1$ and $\mu = 0$). The initial conditions are $\Theta(x, 0) = 0$ and the BC is $\Theta(-1, t) = \sin(4\pi t)^2$. A sinusoidal wave propagates from the left to the right of the interval. The collocation points are shown on the plots ($N = 65$, $\Delta t = 5 \times 10^{-3}$).

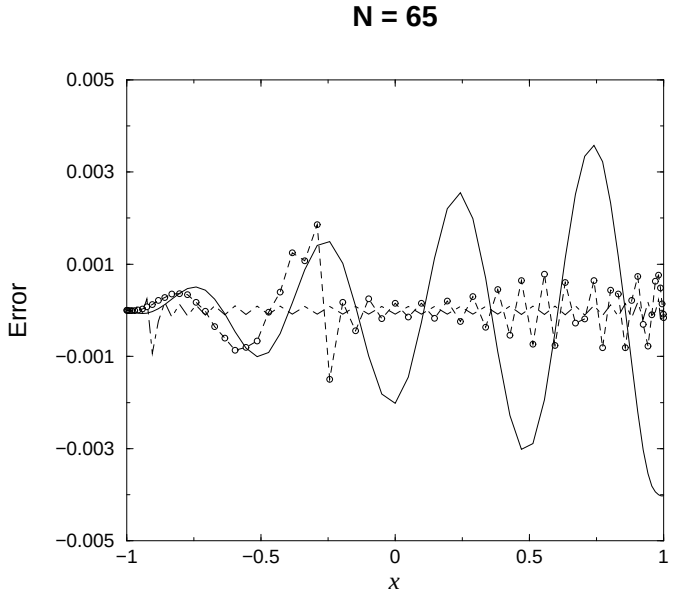

Fig. 4. Profiles at different time steps of the error of the numerical solution shown in Fig. 3. A Gibbs phenomenon appears when the wave is not arrived at the end of interval yet (see text).

has crossed the right boundary. In the present case, $N = 65$ and $\Delta t = 5 \times 10^{-3}$.

When the solution is $\mathcal{C}^\infty$, the error is due to the temporal scheme which is

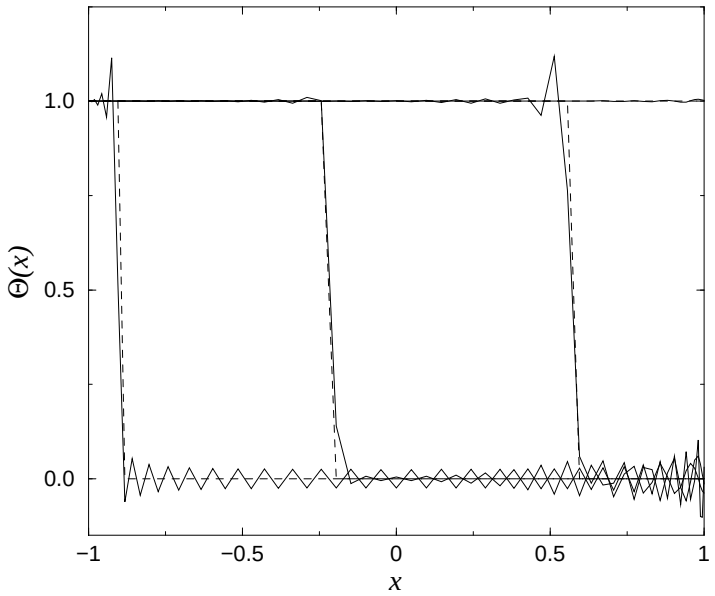

Fig. 5. Profile at different time steps of the Heaviside wave propagating from the left to the right and computed by means of Lanczos approximation. The solid line is the numerical solution and the dashed line the exact one.

a second order implicit one. Decreasing Δt by a factor 2 reduces the error by a factor 4. From Fig. 4, it appears that the error increases linearly as the wave propagates. This is due to the implicit scheme which introduces a dissipative term, which gives an error on the amplitude of the wave. An explicit leap-frog scheme would avoid this drawback. However, whereas it is possible to use a leapfrog temporal scheme for Fourier expansion, such a scheme is unconditionally unstable for Chebyshev expansion (see [21] p. 109). Note that with $N = 21$, the error due to the computation of the spatial derivative is still less than the one due to the temporal scheme when the solution becomes $\mathcal{C}^\infty$.

We conclude that implicit methods should be avoided for solving hyperbolic equations when the phase must be computed with a high accuracy. Finally, it is interesting to compare the above results with the one obtained with finite difference methods. Such a comparison can be found in [21] p. 135. Unfortunately, these authors compare the results obtained with SM versus that obtained by finite difference methods by means of the $\mathcal{L}_2$ error and, therefore, do not give the error on the phase and amplitude of the wave.

In the second example, we compare the solutions obtained with the the Lanczos and dual Lanczos approximations and study the effect of the spectral viscosity. Let us consider again the advection equation with same initial condition $\Theta(x, 0) = 0$ but with a sudden excitation at $x = -1$. The solution is a Heaviside function traveling from the left to the right.

Figure 5 shows the solution computed with the Lanczos approximation. Note

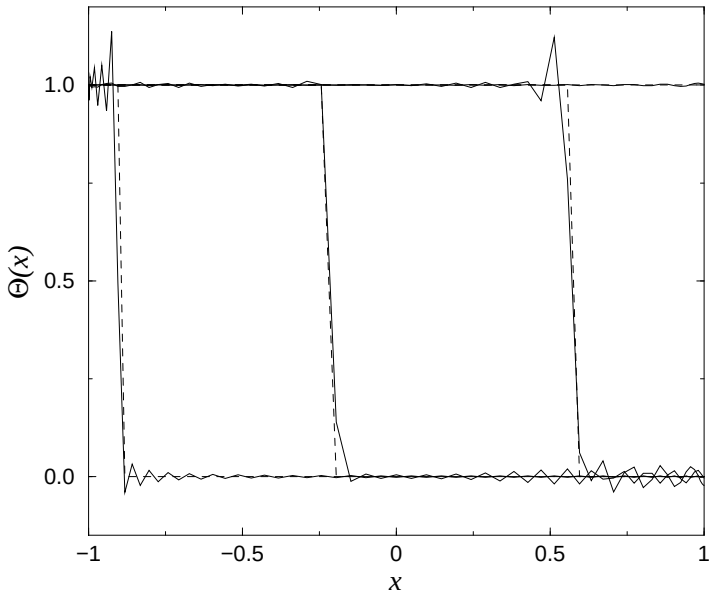

Fig. 6. Same as in Fig. 5 but with the dual Lanczos approximation.

that, in spite of a strong Gibbs phenomenon, the propagation velocity is correctly computed. Figure 6 shows the solution computed with the dual Lanczos approximation (Sect. 4.4). The Gibbs phenomenon is much less important. Figure 7 shows the effect of the spectral viscosity (Sect. 4.6) (we have used a viscosity operator equivalent to $\mathcal{V}^2$). The apodisation effect of the spectral viscosity is well visible. Note that, in spite of the spectral viscosity, the velocity of the front wave is still accurately computed.

5.2 Boundary layers and non local boundary conditions

In this section we give some result obtained by solving the equation (26) in order to show how a boundary layer can be described by means of SM and to show how non local BC works. Fig. 8 shows the solution at different time steps of the equation (26) with $v(x) = 1$ and $\mu(x) = .01$. The initial conditions are the same as in the previous example: $\Theta(x, 0) = 0$. We suddenly switch the left BC to the value 1. The other BC is $\Theta(1, t) = 0$. The Lanczos approximation is used. The different plots of Fig. 8 show the wave propagating from the left to the right. The solution is similar to the one showed for the advection equation but, because of the diffusivity, the wave front is less stiff than in the case of pure advection. When the wave reaches the boundary, the layer is formed. Its thickness is of the order of $2/N_p = 10^{-2}$. Figure 9 shows the comparison between the solution fulfilling the above BC (solid line) and that with a non-local BC (dashed line). The coordinate x was rescaled in order to show the structure of the boundary layer. The BC are $\Theta(-1, t) = 1$ and the second one was chosen in order to minimize the sum of the square of the last

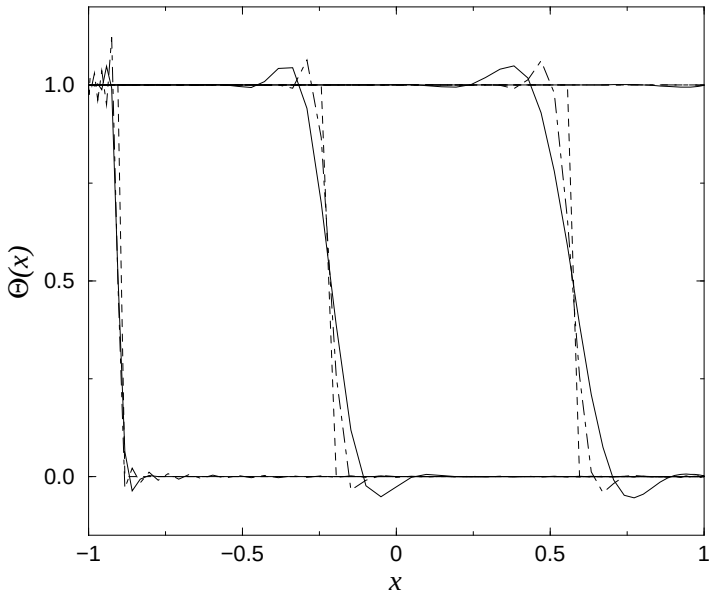

Fig. 7. Same as in Fig. 5 but with dual Lanczos approximation and spectral viscosity. The two profiles, beside the analytical solution (dashed line), correspond to two different values of the spectral viscosity. Note that the discontinuity is smeared out. In spite of the strong spectral diffusivity, the velocity of propagation of the shock is still correctly computed.

three coefficients of the solution. Note that the new solution differs only inside the boundary layer ($0.97 < x \leq 1$). The difference between the two solutions is $\sim 1 \times 10^{-12}$ for $x < 0.5$. With a non local BC, the numerical stability is achieved for any value of $\mu \geq 0$.

5.3 Kompaneets equation and space compactification

The last example is the resolution of the Kompaneets equation ([41]). This equation describes the evolution of the photon distribution function in a bath of plasma at thermal equilibrium at temperature T within the Fokker-Planck approximation (see e.g. [41]). The Kompaneets equation reads:

$$\frac{\partial \mathcal{N}}{\partial t} = \frac{\partial}{\partial \nu}\left[\nu^2 \beta \frac{\partial \mathcal{N}}{\partial \nu} - 2\beta\nu\mathcal{N} + \nu^2\mathcal{N} + \mathcal{N}^2\right] , \tag{37}$$

where $\mathcal{N}(\nu, t)$ is the photon density (function of the frequency ν ($0 \leq \nu < \infty$) and the time t) and β is the plasma temperature in adimensional units. Its asymptotical solution is the Bose distribution:

$$\mathcal{N}(\nu, \infty) = \frac{\nu^2}{\exp(\nu/\beta + \mu) - 1} , \tag{38}$$

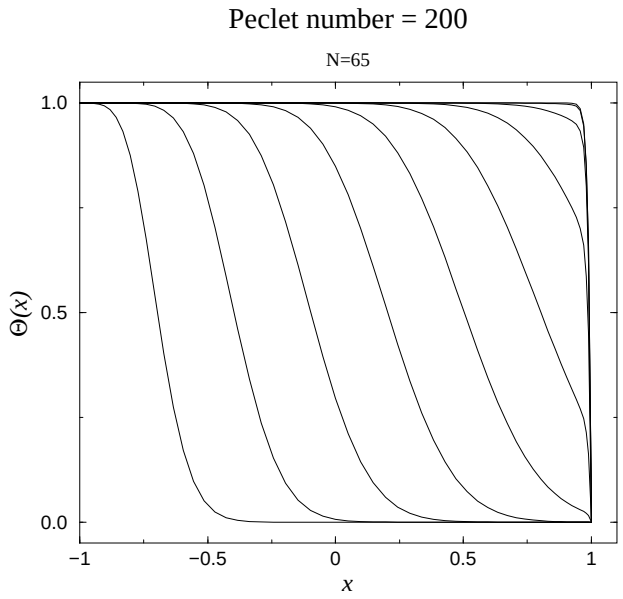

Fig. 8. Profiles at different times of the solution of Eq. (26). Note the formation of the boundary layer near $x = +1$ (N=65, $v(x) = 1$, $\mu(x) = .01$, $N_p = 200$, $\Delta t = .015$).

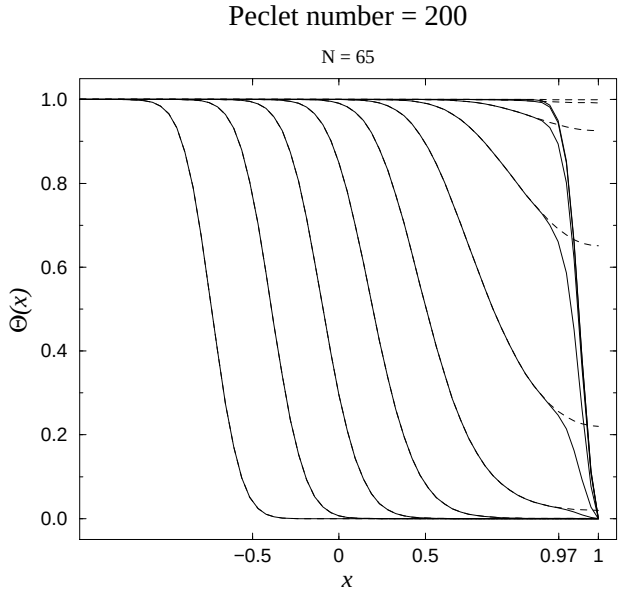

Fig. 9. Same as in Fig. 8 with different boundary conditions. The full line is the solution of with two local B.C. and the dashed one is the solution with a non-local B.C. The x axis has been scaled in order to show the structure of the boundary layer.

where $\mu \geq 0$ is the chemical potential. It is obvious that the Kompaneets equation preserves the number of the photons. If the photon density becomes larger than a critical value, then the photons condense at the frequency $\nu = 0$ (Bose condensation).

To solve the Kompaneets equation, it turns out to be convenient to compactify the frequency space. This compactification can be performed by means of a new variable $x = (\nu-1)/(\nu+1)$ ($x \in [-1,1]$, $\nu = (1+x)/(1-x)$). Equation (37) then becomes

$$\frac{\partial \mathcal{N}}{\partial t} = \frac{4\beta\nu^2}{(1+\nu)^4}\frac{\partial^2 \mathcal{N}}{\partial x^2} + \frac{2}{(1+\nu)^2}\left[\nu^2 + 2\mathcal{N} - \frac{2\nu^2\beta}{1+\nu}\right]\frac{\partial \mathcal{N}}{\partial x} + 2(\nu-\beta)\mathcal{N} \ . \tag{39}$$

If $\mathcal{N}(-1,0) = \mathcal{N}(1,0) = 0$, then $\mathcal{N}(-1,t) = \mathcal{N}(1,t) = 0$ for all $t \geq 0$ and the coefficients of the derivatives vanish at the boundaries $x = -1$ and $x = 1$. Therefore, no BC are required. Moreover, the Courant conditions are fulfilled for $\Delta t \propto 1/N^2$ and implicitation is not necessary.

6 3-D decomposition in spherical coordinates

Spectral methods are well suited to handle the pseudo-singularities tied to spherical-like coordinates (r,θ,ϕ) at $r = 0$ and $\sin\theta = 0$. The various scalar, vector and tensor fields involved in any physical problem cannot be any arbitrary function of these coordinates. Any quantity has to satisfy the so-called *regularity conditions* on the axis $\sin\theta = 0$ and at the origin $r = 0$. These regularity conditions can be taken into account if an appropriated basis of spectral expansion is chosen. Even if *regularity conditions* cannot be called *boundary conditions*, this method to handle pseudo-singularities can be compared to the Galerkin approximation.

As an example, let us consider a scalar function $f(t,r,\theta,\phi)$, with $r \in [0,1]$, $\theta \in [0,\pi]$, and $\phi \in [0,2\pi[$ where (r,θ,ϕ) are the usual spherical coordinates. Assuming that f is a regular scalar function means, in the context of the spectral approximation, $f \in \mathcal{C}^\omega$, that is :

$$f = \sum_{i,j,k} a_{ijk}\, x^i y^j z^k \ , \tag{40}$$

where

$$x = r\sin\theta\cos\phi \ , \quad y = r\sin\theta\sin\phi \quad \text{and} \quad z = r\cos\theta \ . \tag{41}$$

are the usual Cartesian coordinates. Now, substituting (41) into (40) shows that f, considered as a function of (r,θ,ϕ), reads

$$f(r,\theta,\phi) = \sum_{j,k,m} a'_{jkm} r^{m+2j+k} \sin^{m+2j}\theta \cos^k\theta \exp(im\phi) \ . \tag{42}$$

In other words, this means that f is (obviously) a periodic function in the ϕ-direction:

$$f(r,\theta,\phi) = \sum_m a_m(r,\theta)\exp(im\phi) \ , \tag{43}$$

where the coefficients $a_m(r,\theta)$ satisfy

$$a_m(r,\theta) = \sin^m\theta \sum_l a_{lm}(r) {P_l}^m(\cos\theta) \ , \tag{44}$$

where ${P_l}^m$ are the associated Legendre functions. The coefficients $a_{lm}(r)$ satisfy

$$a_{lm}(r) = r^l \sum_j a_{jlm} r^{2j} \ . \tag{45}$$

A way to handle the regularity conditions on the axis $\sin\theta = 0$ is to expand the angular part of f in a series of spherical harmonics

$$f(r,\theta,\phi) = \sum_{l,m} a_{lm}(r) {Y_l}^m(\theta,\phi) \ . \tag{46}$$

Such an expansion ensures that any pseudo-singularity involving $\sin\theta = 0$ is automatically handled. Moreover, spherical harmonics are eigenvectors of the Laplacian operator Δ. This property allows easy inversion of this operator which appears in a lot of physical equations (particularly D'Alembertian operator, dissipative terms of hydrodynamics equations, Poisson equation for the gravitational field, see Sect. 7).

However, from a numerical point of view, this expansion is not efficient in the sense that the transformation in the θ-direction is an expansion in associated Legendre functions ${P_l}^m(\cos\theta)$ which requires $\propto N^2$ operations, N being the number of degrees of freedom, compared to $N\log N$ operations in the case of a Fourier transformation (thanks to the FFT algorithm).

Moreover, it is to be noticed that the regularity conditions described above, namely that the coefficients $a_m(r,\theta)$ of the expansion (43) have to vanish on the axis as $\sin^m\theta$, are not necessary to handle the singularities present in the differential operators. More precisely, it is easy to show that any singularity are automatically handled if the coefficients $a_m(r,\theta)$ satisfy

$$a_m(r,\theta) = \sin^{\mathrm{Min}(m,o)}(\theta) \sum_l a_{lm}(r)\cos(l\theta) \ , \tag{47}$$

where o is the order of the differential operator in the θ-direction. The same considerations hold for the expansion in the r-direction.

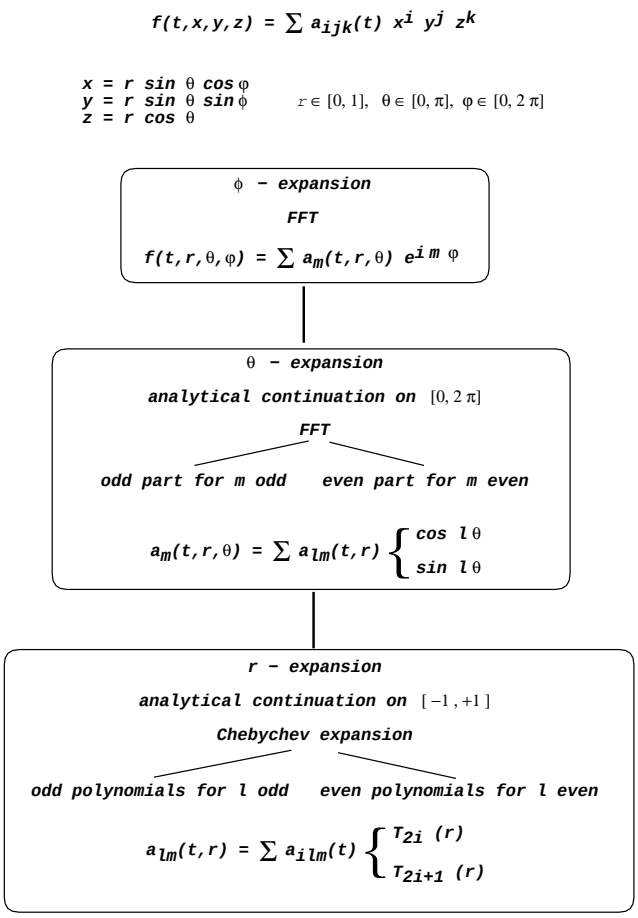

Fig. 10. Expansion of a 3-D scalar function in spherical-like coordinates (r, θ, ϕ).

For these reasons, we expand f as a truncated Fourier series in the ϕ-direction which requires $\propto N_\phi \log N_\phi$ operations. We perform an analytical continuation of the coefficients $a_m(r, \theta)$ on the domain $\theta \in [-\pi, +\pi]$ and expand them in an even (resp. odd) Fourier series in the θ-direction for even (resp. odd) m. This transformation requires $N_\theta \log N_\theta$ operations. The resulting coefficients $a_{lm}(r)$ are analytically continued on the domain $r \in [-1, +1]$ and expanded in a series of even (respectively odd) Chebyshev polynomials depending on the parity of l. This later transformation requires $N_r \log N_r$ operations. The above procedure is detailed in Fig. 10.

7 Scalar Poisson equation in spherical-like coordinates

We will describe methods which are specifically designed to solve PDE which contain scalar and vectorial differential operators in a space domain diffeomorphic to a sphere and in a compactified space. All the numerical algorithms, but one, are fast algorithms. The only exception is the Legendre transformation which requires $\propto N_r \log N_r N_\theta^2 N_\phi \log N_\phi$ instead of $\propto N_r \log N_r N_\theta \log N_\theta N_\phi \log N_\phi$

operations.

7.1 Scalar Poisson Equation in a sphere

Consider the Poisson-like equation in spherical coordinates,

$$\frac{\partial^2\Phi}{\partial r^2} + \frac{2}{r}\frac{\partial\Phi}{\partial r} + \frac{1}{r^2}\left(\frac{\partial^2\Phi}{\partial\theta^2} + \frac{\cos\theta}{\sin\theta}\frac{\partial\Phi}{\partial\theta} + \frac{1}{\sin\theta^2}\frac{\partial^2\Phi}{\partial\phi^2}\right) = S(\vec{x},\Phi,\partial\Phi) \ . \quad (48)$$

Solving by iteration this equation by means of spectral methods in a spherical region is described in [10]. Suppose that the source is known at the $j^{\rm th}$ iteration step. The solution of the Poisson equation at the $(j+1)^{\rm th}$ step can be obtained by solving the following system of ordinary equations on the spherical harmonics coefficients of S, say $S_{lm}(r)$:

$$\left(\frac{d^2}{dr^2} + \frac{2}{r}\frac{d}{dr} - \frac{l(l+1)}{r^2}\right)\Phi_{lm}(r) = S_{lm}(r) \ , \quad (49)$$

where Φ_{lm} are the spherical harmonics coefficients of Φ. The involved Legendre expansion is computed from the Chebyshev expansion in θ by means of a matrix multiplication, as detailed in Appendix A.1 of ref. [16].

Galerkin approximation is used to handle the singularity of Eq.(49) at $r = 0$. For $l = 0$ the solution is expanded on even Chebyshev polynomials $T_{2n}(r)$, $(0 \le r \le 1,\ 0 \le n \le N)$. For l even, the solution is expanded on the set of functions $T_{2n}(r) - T_{2n+2}(r)$. These functions as their first derivative vanish at $r = 0$. An analogous treatment is performed for odd values of l [16]. The matrix representation of the above operator can be easily reduced to a penta-diagonal one. This matrix has a vanishing determinant due to the existence of homogeneous solution $\Phi^{\rm h}_{lm}(r) = r^l$.

The BC are satisfied by adding to a particular solution a homogeneous solution $\Phi^{\rm h}_{ml}$ which must be computed in the coefficient space (see Sect. 4.5). Note that when the source does not depend on ϕ (2-D problems) there exists a fast algorithm for solving the Poisson equation that does not need a Legendre expansion (see Appendix A.2 of [16]). The technical procedure outlined is here is described in details in Sect. 4.5, since the problem is reduced to a one-dimensional one for each value of (l, m).

7.2 Scalar Poisson Equation in a shell

The solution of the Poisson equation in a shell $R_{\rm in} \leq r \leq R_{\rm out}$ is performed in a very similar way. The main differences are: there is no singularity in the coefficients of the radial part of Eq. (49) and there are two homogeneous solutions $\Phi^{\rm h1}_{lm}(r) = r^l$ and $\Phi^{\rm h2}_{lm} = 1/r^{l+1}$. The last analytical homogeneous solution can be used to fulfil the two BC. However, it turns out that better results are obtained by using an homogeneous solution obtained by means of the Lanczos approximation. In practice an aspect ratio $R_{\rm out}/R_{\rm in}$ larger than 2 should be avoided.

7.3 Solution of the Poisson equation in a compactified space

Some of the Einstein equations lead to Poisson equations for which the source $S(r, \theta, \phi)$ fills all the space and vanishes at least as $\propto 1/r^4$ when $r \to \infty$. Noting that the solution can be expanded in power series of the variable $u = 1/r$, it is natural to solve the Poisson equation in two domains D_1 and D_2 defined respectively by $0 \leq r \leq 1$ and $1 \geq u \geq 0$ and to match the two solutions and their derivatives at the common boundary. The radial part of the Poisson operator (with respect to u) in the domain D_2 reads:

$$\Delta_u = u^4 \left(\frac{d^2}{du^2} - \frac{l(l+1)}{u^2} \right) \ . \tag{50}$$

The source must thus be divided by the factor u^4. This division must be performed in the coefficient space in order to avoid the singularity at $u = 0$ and to minimize the roundoff errors. The reader will find all details in [12]. Extension of the above technique for more complicate cases (few domains) are straightforward. Generalization to parabolic equations is also straightforward. On the contrary, the above space compactification cannot be used for the wave equation.

7.4 Poisson equation in a non-spherical domain

Rotating or/and binary stars are not spherical but their surface are diffeomorphic to a sphere. In order to fulfil the BC and to reduce truncation errors, it is useful to introduce a system of coordinates adapted to the geometry of the star. It is easy to find such a coordinates system, at least for star-like domains (cf. [12]). Let $r = F(\theta, \phi)$ be the equation of the surface of the star. Consider

the new coordinate system (ξ, θ', ϕ') defined by [12]

$$r = a\xi + \xi^3 \bar{F}(\theta, \phi) + \xi^4 \hat{F}(\theta, \phi), \quad \theta' = \theta, \quad \phi' = \phi \ , \tag{51}$$

where $\bar{F}$ and $\hat{F}$ are such that (i) $F(\theta, \phi) = a + \bar{F}(\theta, \phi) + \hat{F}(\theta, \phi)$ and (ii) the Fourier expansion of $\bar{F}(\theta, \phi)$ (resp. $\hat{F}(\theta, \phi)$) with respect to ϕ contains only even (resp. odd) harmonics. The property (i) ensures that the surface of the star is given by $\xi = 1$, whereas property (ii) is necessary to have a regular coordinates transformation. Under the coordinates transformation (51), the Poisson equation can be written in the following way:

$$A\, \Delta' \Phi = B^{ik} \frac{\partial^2 \Phi}{\partial x^i \, \partial x^k} + + C^i \frac{\partial \Phi}{\partial x_i} + S(\xi, \theta', \phi', \Phi, \partial \Phi) \ , \tag{52}$$

where Δ' is the ordinary Laplacian with respect to the coordinates $(\xi, \theta' \phi')$ (i.e. Δ' has the same form as the operator (48) when (r, θ, ϕ) are replaced by $(\xi, \theta' \phi')$) and A, B and C are functions of the coordinates $(\xi, \theta' \phi')$. Equation (52) is solved by means of an iterative procedure. Since A is not a constant, a procedure similar to that described in Sect. 4.1 (Eq. (29)) is used. No convergence problems were found. Note that the above method can be inefficient if the source S does not depend on Φ and on its derivatives because the iterative procedure would still be required, whereas the equation would be linear in Φ. However, in the cases of interest, the source S is a non linear function of Φ and of its first derivatives. Therefore an iterative procedure is required anyway. The computing time for solving Eq. (52) is similar to the one for solving Eq. (48).

8 Vectorial equations in spherical-like coordinates

The divergence and curl operators acting on a 3-vector $\vec{V}$ read:

$$\vec{\nabla} \cdot \vec{V} = \frac{\partial V_r}{\partial r} + \frac{1}{r} \left(2\, V_r + \frac{\partial V_\theta}{\partial \theta} + \frac{\cos\theta}{\sin\theta}\, V_\theta + \frac{1}{\sin\theta} \frac{\partial V_\phi}{\partial \phi} \right) \tag{53}$$

and

$$\begin{aligned}
\left[\vec{\nabla} \wedge \vec{V} \right]_r &= \left[\partial_\theta (V_\phi \sin\theta) - \partial_\phi V_\theta \right] / (r \sin\theta) \\
\left[\vec{\nabla} \wedge \vec{V} \right]_\theta &= \left[\partial_\phi \, V_r - \partial_r (r \sin\theta V_\phi) \right] / (r \sin\theta) \\
\left[\vec{\nabla} \wedge \vec{V} \right]_\phi &= \left[\partial_r (r V_\theta) - \partial_\theta \, V_r \right] / r \ ,
\end{aligned} \tag{54}$$

where $V_r,\ V_\theta,\ V_\phi$ denote the components of a $\vec{V}$ with respect to the orthonormal basis $(\partial_r,\ 1/r\ \partial_\theta,\ 1/(r\sin\theta)\ \partial_\phi)$ associated with spherical coordinates (r, θ, ϕ).

It is worth to note a typical behaviour of the spherical components of a vector. Consider a constant vector $\vec{V}$ whose Cartesian components are $V_x = 1,\ V_y = 0,\ V_z = 0$. The corresponding spherical components are $V_r = \sin\theta\cos\phi,\ V_\theta = \cos\theta\cos\phi,\ V_\phi = -\sin\phi$. From the expression of the divergence (53), it is easy to see that there are three singular terms at $r = 0$ and $\theta = 0, \pi$ while the sum of these terms is regular. This is due to the fact that the spherical components of a well behaved vector are not independent.

A way to overcome this problem is to compute and to add the terms which generate the singularity before dividing by r and $\sin\theta$ and to perform the division on the sum. Performing these operations in the coefficient space allows to resolve the indeterminations at the singular points and to reduce the roundoff errors. Another method consists in subtracting to $\vec{V}$ the constant component whose divergence vanishes. This decomposition can be easily done in the coefficient space.

8.1 Vector decomposition

The Clebsch theorem states that a vector $\vec{V}$ can be uniquely decomposed into a sum of a divergence-free vector $\vec{W}$ and a curl-free vector $\vec{\nabla}\,\Phi$. This decomposition results from the resolution of a Poisson equation: the divergence of $\vec{V} = \vec{W} + \vec{\nabla}\,\Phi$ gives indeed $\Delta\Phi = \vec{\nabla}\cdot\vec{V}$, which has to be solved to get Φ. $\vec{W}$ is then computed according to $\vec{W} = \vec{V} - \vec{\nabla}\Phi$. The above primitives are computed according to the method exposed in Sect. 3.2. Once a particular solution $\vec{W}_{\rm p}$ is obtained, a more general solution satisfying the desired BC can be obtained by adding to $\vec{W}_{\rm p}$ an homogeneous solution $\vec{W}_{\rm h} = \vec{\nabla}\,\Phi_{\rm ha}$ were $\Phi_{\rm ha}$ is an harmonic function.

8.2 Solution of the equation $\vec{\nabla}\wedge\vec{V} = \vec{S}$

The curl operator $\vec{\nabla}\wedge$ being degenerated, the vectorial equation $\vec{\nabla}\wedge\vec{V} = \vec{S}$ can be solved only if the divergence of $\vec{S}$ vanishes (integrability condition). Because of this degeneracy, we can seek for a particular solution $\vec{V}_0$ for which one component vanishes.

Taking for example $V_r = 0$, the second equation of the system (54) $\vec{\nabla}\wedge\vec{V} = \vec{S}$ becomes $\partial_r\,(r\,V_\phi) = -r\,S_\theta$ from which we get $V_\phi = -\frac{1}{r}\int_0^r r' S_\theta dr'$. In the same way, we get $V_\theta = \frac{1}{r}\int_0^r r' S_\phi dr'$. Once this particular solution is obtained, we

can add to it the gradient of some scalar function in order to obtain a more general solution satisfying the desired BC.

8.3 Vectorial Poisson Equation

The Einstein equations lead to a vectorial Poisson equation for the shift vector (Eq. (69) below):

$$\Delta\vec{V} + \lambda\vec{\nabla}(\vec{\nabla}\cdot V) = \vec{S}\ , \tag{55}$$

where λ is some constant. Noting that $\Delta \equiv -\vec{\nabla}\wedge\ \vec{\nabla}\wedge + \vec{\nabla}\,\vec{\nabla}\cdot$, Eq. (55) can be written as

$$-\ \vec{\nabla}\wedge\ \vec{\nabla}\wedge\vec{V} + (\lambda+1)\vec{\nabla}(\vec{\nabla}\cdot\vec{V}) = \vec{S}\ . \tag{56}$$

We shall show how to find the solution of (56) in the spherical domain ($0 \leq r \leq 1$). Let us first consider the degenerated case $\lambda = -1$. The integrability condition is $\vec{\nabla}\cdot\vec{S} = 0$. Let us introduce the vector $\vec{P} = \vec{\nabla}\wedge\vec{V}$ which obeys to $\vec{\nabla}\wedge\vec{P} = \vec{S}$. Following the method described in Sect. 8.2, we can solve this last equation and get $\vec{P} = \vec{P}_{\rm p} + \vec{\nabla}(\Psi + \Psi_{\rm ha})$ where $\vec{P}_{\rm p}$ is a particular solution, Ψ an arbitrary function and $\Psi_{\rm ha}$ an harmonic function which can be used to fulfil the BC. The integrability condition imposes that $\Delta\Psi = -\vec{\nabla}\cdot\vec{P}_{\rm p}$. The final equation for $\vec{V}$ is $\vec{\nabla}\wedge\vec{V} = \vec{P} + \vec{\nabla}(\Psi + \Psi_{\rm ha})$. A particular solution $V_{\rm p}$ of this equation (for $\Psi_{\rm ha} = 0$) can be obtained by means of the method described in Sect. 8.2. The vector $\vec{V}_{\rm g} = \vec{V}_{\rm p} + \vec{\nabla}\Xi$, where Ξ is some arbitrary function, is again a solution of (55) but is not the most general one. Actually, we can add to it any solution of $\vec{\nabla}\wedge\vec{V}_{\rm ha} = \vec{\nabla}\Psi_{\rm ha}$. Such a solution can easily be obtained by means of a spherical harmonics expansion of $\Psi_{\rm ha}$.

The case $\lambda \neq -1$ can be reduced to the previous one. Let us introduce $\vec{V} = \vec{W} + \vec{\nabla}\Phi$ and apply the vector decomposition as described in section 8.1 to the source. Φ can be computed by means of the divergence of both sides of Eq. (55). Now, the divergence-free counterpart $\vec{W}$ can be computed as in the previous case ($\lambda = -1$).

The methods described above to solve Poisson equations cannot be generalized to the parabolic or hyperbolic case. Consider the equation (telegraph equation)

$$\alpha\frac{\partial^2\vec{V}}{\partial\, t^2}+\beta\frac{\partial\vec{V}}{\partial t}+\lambda\vec{\nabla}(\vec{\nabla}\cdot\vec{V})+\Delta\vec{V}=\vec{S}\ , \tag{57}$$

where α, β and λ are arbitrary constants. After decomposition of the source into a curl-free and a divergence-free component, the problem can be split in two parts. This is done mainly in solving a scalar telegraph equation for the curl-free component and a vectorial (with $\lambda = 0$) telegraph equation for the divergence-free part.

Eq. (57) explicitely reads:

$$\begin{aligned}
&D_tV_r+\frac{\partial^2V_r}{\partial r^2}+\frac{4}{r}\frac{\partial V_r}{\partial r}+\frac{1}{r^2}\left(2\,V_r\frac{\partial^2V_r}{\partial\theta^2}+\frac{\cos\theta}{\sin\theta}\frac{\partial V_r}{\partial\theta}+\frac{1}{\sin\theta^2}\frac{\partial^2V_r}{\partial\phi^2}\right)\\
&\qquad-\frac{2}{r}\nabla\cdot\vec{V}=S_r \qquad (58)\\
&D_tV_\theta+\frac{\partial^2\,V_\theta}{\partial r^2}+\frac{2}{r}\frac{\partial V_\theta}{\partial r}+\frac{1}{r^2}\left(\frac{\partial^2V_\theta}{\partial\theta^2}+\frac{\cos\theta}{\sin\theta}\frac{\partial\,V_\theta}{\partial\theta}+\frac{1}{\sin\theta^2}\frac{\partial^2V_\theta}{\partial\phi^2}\right)\\
&\qquad+\frac{1}{r^2}\left(2\,\frac{\partial\,V_r}{\partial\theta}-2\,\frac{\cos\theta}{\sin\theta}\,\frac{\partial V_\phi}{\partial\phi}-\frac{V_\theta}{\sin\theta^2}\right)=S_\theta \qquad (59)\\
&D_tV_\phi+\frac{\partial^2V_\phi}{\partial r^2}+\frac{2}{r}\frac{\partial V_\phi}{\partial r}+\frac{1}{r^2}\left(\frac{\partial^2V_\phi}{\partial\theta^2}+\frac{\cos\theta}{\sin\theta}\frac{\partial\,V_\phi}{\partial\theta}+\frac{1}{\sin\theta^2}\frac{\partial^2V_\phi}{\partial\phi^2}\right)\\
&\qquad+\frac{1}{r^2\sin\theta}\left(\cos\theta\,\frac{\partial\,V_\phi}{\partial\theta}+2\,\frac{\partial\,V_r}{\partial\phi}+\frac{2\cos\theta}{\sin\theta}\,\frac{\partial V_\theta}{\partial\phi}-\frac{V_\phi}{\sin\theta}\right)=S_\phi\ , \qquad (60)
\end{aligned}$$

where we have introduced $D_t\vec{V}\stackrel{def}{=}\alpha\,\partial^2\vec{V}/\partial\,t^2+\beta\,\partial\vec{V}/\partial t$. It easy to see that these equations are badly coupled. Moreover, there is a lot of singular terms (cf. Sect. 8). The first equation is coupled with the others by $\vec{\nabla}\cdot\vec{V}$. Consequently, seeking for a divergence-free solution to the equation for V_r reduces to a telegraph equation and can be solved *mutatis mutandis* by means of the method described in [5]. Once V_r is known, we can seek for a solution of the system of coupled equation governing $V_\theta,\ V_\phi$ whose sources are

$$\begin{aligned}
&\hat{S}_\theta=S_\theta-2/r^2\,\partial_\theta V_r\\
&\hat{S}_\phi=S_\phi-2/(r\sin\theta)^2\,\partial_\phi V_r\ . \qquad (61)
\end{aligned}$$

Introducing the couples of potentials (Λ, Υ) and (U, W), defined by

$$\frac{1}{r}\left[\frac{\partial\,\Lambda}{\partial\theta} - \frac{1}{\sin\theta}\,\frac{\partial\Upsilon}{\partial\phi}\right] = \hat{S}_\theta, \quad \frac{1}{r}\left(\frac{1}{\sin\theta}\,\frac{\partial\Lambda}{\partial\phi} + \frac{\partial\Upsilon}{\partial\theta}\right) = \hat{S}_\phi \tag{62}$$

$$\frac{1}{r}\left(\frac{\partial\,U}{\partial\theta} - \frac{1}{\sin\theta}\,\frac{\partial\,W}{\partial\phi}\right) = V_\theta, \quad \frac{1}{r}\left(\frac{1}{\sin\theta}\,\frac{\partial U}{\partial\phi} + \frac{\partial W}{\partial\theta}\right) = V_\phi \tag{63}$$

allows to decouple Eqs. (59) and (60).

Assume that the functions Λ and Υ are known by means of the resolution of the system (62,63). After some algebra, a solution of the telegraph equation (57) can be obtained by solving the associated equations

$$\begin{aligned} D_t U + \tilde{\Delta} U &= \Lambda \\ D_t W + \tilde{\Delta} W &= \Upsilon\ , \end{aligned} \tag{64}$$

where

$$\tilde{\Delta} \equiv \frac{\partial^2}{\partial r^2} + \frac{1}{r^2}\left(\frac{\partial^2}{\partial\,\theta^2} + \frac{\cos\theta}{\sin\theta}\frac{\partial}{\partial\theta} + \frac{1}{\sin\theta^2}\,\frac{\partial^2}{\partial\phi^2}\right) \tag{65}$$

It remains now to find the sources Λ and Υ of the system (64). Taking the angular divergence of $\hat{S}_\theta$ and $\hat{S}_\phi$ allows to transform the system (61) as

$$\Delta_{\theta,\phi}\,\Lambda = \frac{\partial\hat{S}_\theta}{\partial\theta} + \frac{\cos\theta}{\sin\theta}\,\hat{S}_\theta + \frac{1}{\sin\theta^2}\frac{\partial\hat{S}_\phi}{\partial\phi}\ , \tag{66}$$

where $\Delta_{\theta,\phi}$ is the angular part of the ordinary Laplacian. This last equation can be easily solved by means of a Fourier-Legendre transformation. Once Λ is known, Υ can be easily computed.

It is to be noticed that the use of Cartesian components $V_x,\ V_y,\ V_z$ would greatly simplify the resolution of the telegraph equation. The drawback of this short cut is that only some simple classes of BC can be easily implemented (e.g. $V_r = V_\theta = V_\phi = 0$). For more general BC, spherical components of $\vec{V}$ and $\vec{S}$ must be used. Finally, let us mention that the above method can be used to solve the vectorial Poisson equation too, since it is a special case of Eq. (57), obtained by setting α, β and λ to zero. This integration method was used to solve a vectorial Poisson equation in studying the bifurcation points of general relativistic rotating neutron stars [5] (cf. Sect. 9.9 below).

9 Astrophysical applications

9.1 Einstein equations

In this section we give for completeness a short outline of the Einstein equations [53], [58], [59]. This section is not strictly necessary to understand the following ones, and the reader that does not have some background of differential geometry can skip it.

Einstein equations describe the evolution of the metric $g_{\alpha\beta}$ of a 4-D Riemannian manifold (Greek indices α, β run from 0 to 3, Latin indices i, j run from 1 to 3, $x^0 = ct$). It is convenient to write the distance element ds^2 on the following form:

$$ds^2 = -\alpha^2 (dx^0)^2 + \gamma_{ij}(dx^i - \beta^i dt)(dx^j - \beta^j dt) \ . \tag{67}$$

The 10 Einstein equations (1) are not independent because of the Bianchi identities (2). Therefore there is the possibility to impose 4 gauge conditions. If the *maximum slicing* and *minimal distortion* gauge is chosen (cf. [53]), the Einstein equations (1) can be written in the following symbolic way (where we have introduce the Cartesian components of γ_{ij})

$$\Delta\alpha = \rho + Q_0 \tag{68}$$

$$\Delta\beta_i + \frac{1}{3}\nabla_i \nabla_j \beta^j = S_i + Q_i \tag{69}$$

$$\Delta \log\gamma = P + \bar{Q} \tag{70}$$

$$\frac{1}{c^2}\frac{\partial^2 \gamma_{ik}}{\partial t^2} - \Delta\gamma_{ik} = P_{ik} + Q_{ik} \ , \tag{71}$$

where γ is the determinant of the space metric γ_{ik}, ρ, S_i, P and P_{ik} are related to the matter energy momentum tensor $T_{\alpha\beta}$, Δ is the ordinary flat-space Laplacian and Q_0, Q_i, $\bar{Q}$ and Q_{ik} represent a formal source containing all the non-linear terms of the Einstein equations. It is easy to see that the first five equations are elliptical, the other ones are hyperbolic. The above equations can simplify enormously if some symmetries are present. For example, in spherical symmetry, a non-static solution of the system (68)-(71) can be found by solving a system of two PDEs for the metric and two PDEs for the matter. An axial symmetric circular steady state solution can be found by solving a systems of 4 elliptical equations [14]. The problems becomes more complicated in the noncircular case. In this case, in spite of the axial symmetry, all the 10 equations of the system must be solved [24]. In the next sections we shall describe some astrophysical applications obtained by our group by solving the Einstein equations (68)-(71).

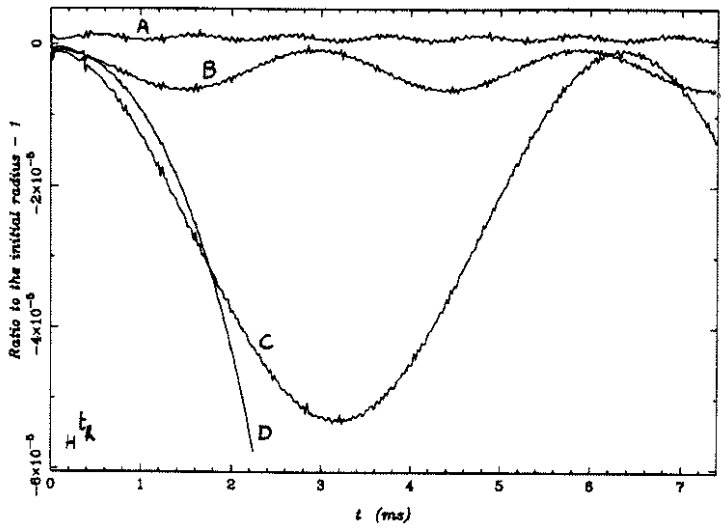

Fig. 11. Time evolution of the stellar radius for four initial configurations close to the neutron star maximum mass [23]. The relative differences with the maximum mass are respectively -3.3×10^{-3}, -5.0×10^{-5}, -3.6×10^{-6} and -3.8×10^{-6} for configurations labelled A, B, C and D. The models A, B and C are on the stable branch of the mass-central density curve, whereas model D is on the unstable branch. Note that the high frequency small oscillations are real and corresponds to stable acoustic modes. They keep the same amplitude and same frequency for the four configurations. On the contrary, the real part of the frequency of the unstable Jeans mode tends to zero along the sequence A, B, C and its amplitude increases. For configuration D the frequency becomes imaginary, leading to a collapse (not shown on the figure for the benefit of presentation).

9.2 1-D gravitational collapse of a neutron star towards a black hole

Accreting neutron stars (e.g. in X-ray binary systems) can reach the maximum mass allowed by general relativity [46], which marks the stability limit against radial perturbations [30]. Any subsequent accretion will trigger the collapse towards a black hole. This phenomenon may be an important source of neutrinos [25]. We have studied the collapse by means of a general relativistic and spherically symmetric hydrodynamical code [22], [23]. The initial configurations were solutions of the hydrostatic equations (Tolmann-Oppenheimer-Volkoff equations). The high accuracy of spectral methods allows to take initial stable configurations, the mass of which differs from the critical mass by a few 10^{-6} solar mass. The numerical round-off error cause the solution not to remain exactly static. It performs instead gentle oscillations of relative amplitude 10^{-10} except for the fundamental mode, which grows exponentially for initial unstable configurations (cf. Fig 11). The collapse is then computed up to the formation of an apparent horizon which leads to a coordinate singularity [22].

9.3 1-D gravitational collapse within tensor-scalar gravitational theory

We have recently studied the gravitational wave emission from 1-D gravitational collapse by solving the complete tensor-scalar and hydrodynamic equations for a self-gravitating perfect fluid [43,44]. The initial conditions describe unstable-equilibrium neutron star configuration. In the case of shock formation, we have coupled our Poisson code to a Godunov-type solver for the hydro given by Valencia's group [40], [31], [43]. We found that these kind of sources are not likely to be observed by future laser interferometric gravitational wave detectors (such as VIRGO or LIGO) if they are located at more than a few 100 kpc. However, spontaneous scalarization could be constrained if such a gravitational collapse is detected by its quadrupolar gravitational signal since this latter is quite lower than the monopolar one.

9.4 2-D Kerr black hole

We have tested our method for solving the axisymmetric stationary Einstein equations against a non trivial 2-D analytical solution, namely the Kerr solution (see e.g. [56]), which describes rotating black holes. For treating this problem, four equations must be solved: Eq. (68) for α, only one of the three Eqs. (69) (that for β^ϕ) and two equations equivalent to the system (70)-(71). These equations are solved outside the event horizon (given by the (isotropic) radial coordinate $r = 1$) up to infinity, by means of a compactification as explained in Sect. 7.3 [6,5]. The horizon is a singular point for the coefficient of the operator $\frac{\partial}{\partial r}$ in Eq. (69). This problem is a typical Von Neumann-Dirichlet problem. Figure 12 shows the error on the shift β^ϕ for a Kerr black hole with an angular momentum parameter $a/M = 0.99$. Note that for $a/M = 1$ the horizon shrinks to a point, so that the singularity becomes essential.

9.5 2-D magnetized rotating neutron stars

We have developed a numerical code for solving the coupled Einstein-Maxwell equations describing steady states of magnetized rotating neutron stars. From the mathematical point of the view, this problem amounts to solving four non-linear elliptical gravitational field equations, as in Sect. 9.4, one elliptic equation for the magnetic vector potential (the Grad-Shafranov equation) and one elliptic equation for the electric scalar potential. These latter two equations are coupled to the gravitational field ones via the metric tensor. The steady-state configuration of the fluid is obtained by using a first integral of motion [3]. This code has been applied to compute the magnetic field induced distortion of rotating neutron stars (Figs. 13 and 14) in order to estimate the

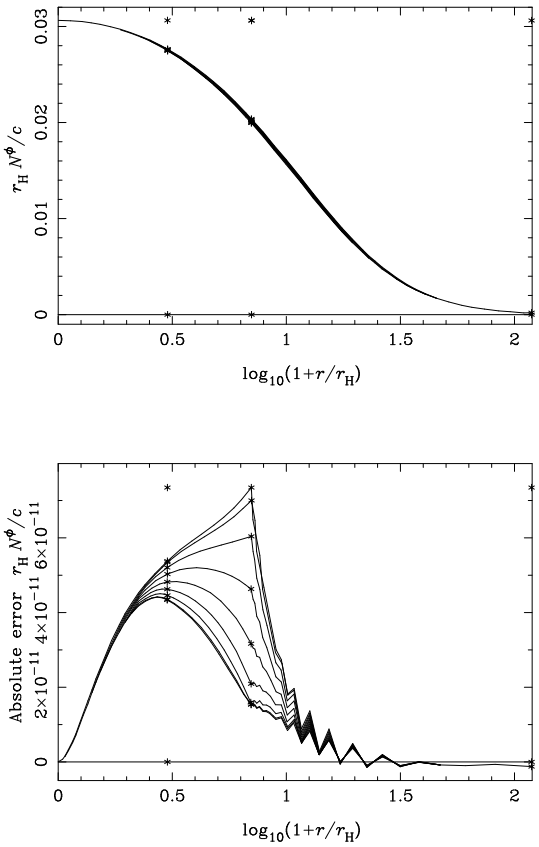

Fig. 12. Shift vector component β^ϕ (top) and error with respect to the analytical solution (bottom) for a Kerr black hole with angular momentum parameter $a/M = 0.99$ [5]. The different curves corresponds to different values of the θ angle. The asterisks indicate sub-domain boundaries.

resulting gravitational radiation [7]. Note that a direct comparison study has been conducted between the spectral code and two codes based on different methods (finite differences) in the case of non-magnetized rapidly rotating neutron stars [45].

9.6 2-D hot new born neutron star

We have computed models of differentially rotating proto-neutron stars using realistic equations of state of dense hot matter in the framework of general relativity [27] [28]. We found a minimum period of uniform rotation of cooled neutron stars which formed directly (i.e. without a subsequent significant accretion of mass) from proto-neutron stars with shocked envelope of about 1.7 ms. This strengthens the hypothesis that millisecond pulsars are accretion accelerated neutron stars.

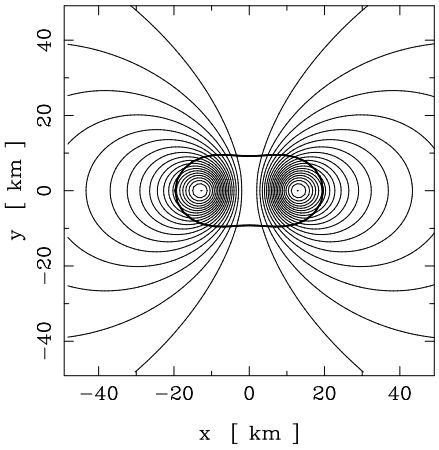

Fig. 13. Magnetic field lines and surface of the star (thick line) for a neutron star deformed by a huge magnetic pressure [3].

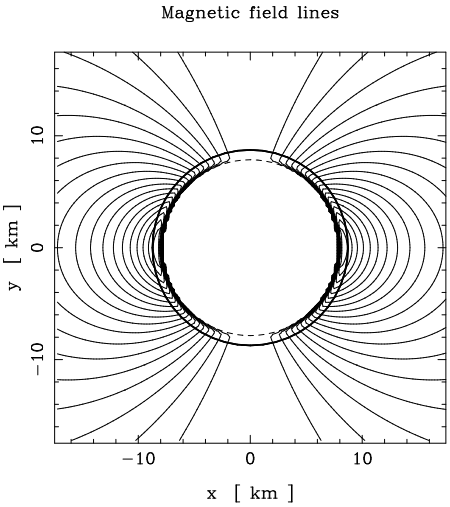

Fig. 14. Magnetic field lines and surface of the star (thick line) for a realistic magnetized neutron star, with superconducting interior [7].

9.7 3-D stellar core collapse

A fully 3-D hydrodynamical Newtonian code for self-gravitating bodies has been developed within spectral methods and employed to compute the gravitational wave emission from the infall phase of a type II supernova [17]. The initial conditions are self-consistent configurations of rotating stellar cores embedded in the tidal field of a companion, hence are fully triaxial. They are computed by means of an iterative procedure.

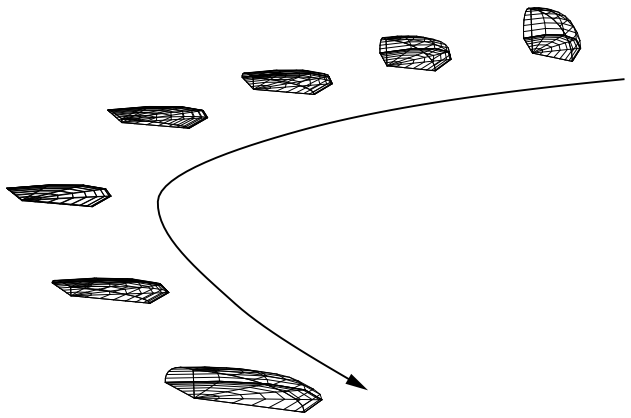

Fig. 15. Shape of the grid (adapted to the star) at different times during a close encounter with a massive black hole (the grid is initially the fourth of a sphere) [39]. This computation has been performed with only 17 degrees of freedom in r, 9 in θ and 8 in ϕ.

9.8 3-D tidal disruption of a star by a massive black hole

We have studied the close encounter of a star and massive black hole, possibly at the centre of a galaxy [39]. Tidal forces compress dramatically the star, as shown in Figs. 15 and 16. This phenomenon has been proposed as a possible mechanism for gamma-ray burst generation [19]. The 3-D Euler equations are solved in the external field of the black hole. As already said in Sect. 1, this application demonstrates the capability of SM in computational resource saving.

9.9 Spontaneous symmetry breaking of a rapidly rotating neutron star

We have computed the location of the bifurcation point between (axisymmetric) MacLaurin-like and (triaxial) Jacobi-like configurations along sequences of rapidly rotating stars in the framework of general relativity [4,5]. To tackle this problem, we solved Eq. (68), the three Eqs. (69) (by means of the technique described in Sect. 8.4), and two equations like (69) and (71). The gravitational radiation is neglected. The matter distribution is obtained thanks to a first integral of motion and depends on the equation of state of nuclear matter. Such mechanism can be a powerful source of continuous gravitational waves from accreting neutron stars in binary systems [8,9].

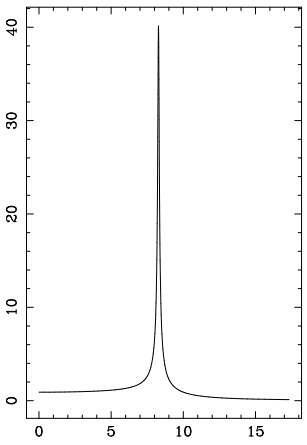

Fig. 16. Time evolution of the central density of star during its trip around a massive black hole [39].

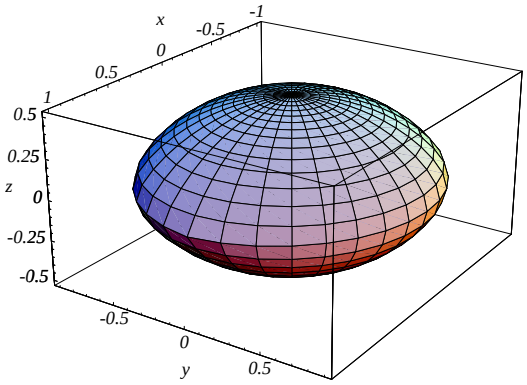

Fig. 17. Rapidly rotating neutron star, which has become triaxial due to the viscosity driven instability [4,5]. The ellipticity in the equatorial plane is about 0.1. Notice the cusp at the stellar equator in direction of the semi-major axis (x–axis), where the rotation is Keplerian, and which is absent along the semi-minor axis (y–axis).

9.10 Close binary systems of compact objects

We have developed a numerical code for computing quasi-equilibrium configurations of relativistic binary systems [12]. This code is based on a *multi-domain spectral method*, i.e. the whole space is divided into various domains and a spectral method is used in each domain, as described in Sect. 7. The external domain extends to infinity thanks to some compactification. The boundaries of each domain are chosen in order to coincide with physical limit surfaces,

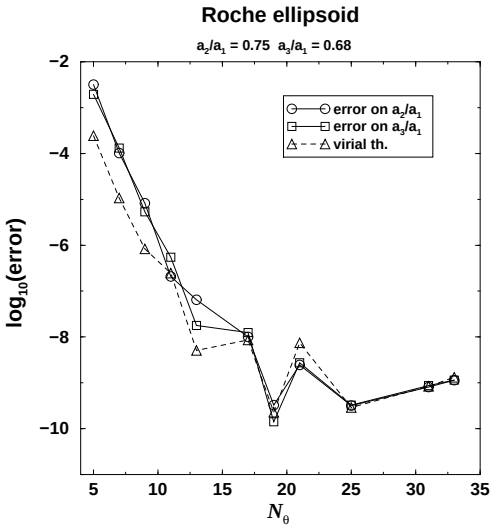

Fig. 18. Logarithm of the relative global error of the numerical solution with respect to the number of degrees of freedom in θ for a Roche ellipsoid for an equal mass binary system and $\Omega^2/(\pi G\rho) = 0.1147$ (the numbers of degrees of freedom in the other directions are $N_r = 2N_\theta - 1$ and $N_\varphi = N_\theta - 1$) [12]. Also shown is the error in the verification of the virial theorem.

such as the surface of a star (cf. Sect. 7.4). In this manner, the physical discontinuities in some fields or their derivatives are located at the boundary of the domains and the applied spectral methods are free of any Gibbs-phenomenon, resulting in a very high precision. We use a spherical-type coordinate system (r', θ', ϕ') which maps the physical domain to the unit sphere. This technique is able to treat any physical boundary which is starlike; this includes any realistic shape taken by the surface of a rotating neutron star in a tidal field. Among the tests passed by the code, the comparison with analytic solutions (MacLaurin and Roche ellipsoids) shows that the achieved precision is of the order 10^{-10} (cf. Figure 18). The final stages of NS binaries are expected to be irrotational with respect to an inertial frame (see [11] and references therein). This means that when seen in the co-orbiting frame, each star is counter-rotating with respect to the orbital motion. The velocity field with respect to the orbiting frame must then to be computed. A typical numerical solution is shown in Fig. 19. The first numerical results about irrotational binary configurations in general relativity have been presented in Ref. [13].

10 Conclusion

We hope to have convinced the reader that spectral methods are a highly valuable tool in the field of relativistic astrophysics. They can lead to results typically several orders of magnitude more accurate than those provided by finite difference methods. This high accuracy is very useful for studying sta-

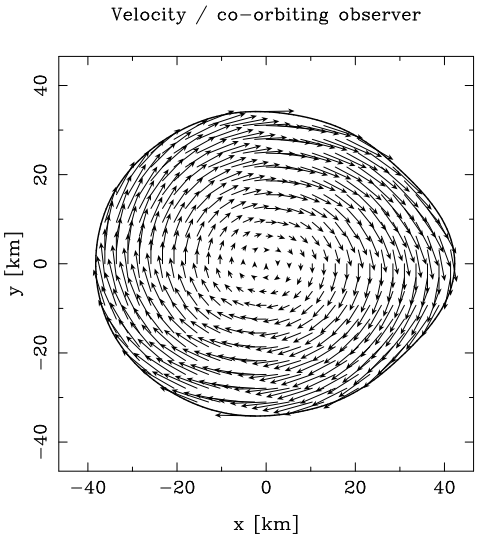

Fig. 19. Velocity field with respect to the orbiting frame, inside a star which is member of a close binary system. The plane of the figure is the orbital plane. The companion is located at the right.

bility problems (Sect. 9.2 and 9.9). Of course, spectral methods have their drawbacks. Let us summarize the advantages and drawbacks from our experience:

- **Advantages:**
  - · very high accuracy for treating smooth fields and their derivatives (evanescent error);
  - · economy of number of degrees of freedom (grid points);
  - · rigorous treatment of boundary conditions;
  - · multi-domain (multi-grid) technique easily implemented without any loss of accuracy;
  - · rigorous treatment of regularity conditions associated with singular coordinates such as spherical coordinates;
  - · efficient algorithms for von Neumann-Dirichlet problems;
  - · modularity;
  - · well developed mathematical theory;
  - · lack of robustness (this is an advantage because no solution can be found for ill-posed problems);
- **Drawbacks:**
  - · spurious oscillations when treating discontinuous fields (Gibbs phenomenon);
  - · severe Courant conditions and therefore need of implicitation (Sect. 4.1);

  Note however that in the 2-D Fourier case, spectral hyperviscosity has proved to be efficient in shock handling [48,47].

Clearly there is no ideal numerical method for treating all the problems and a combination of different methods for solving a given problem may turn out to be fruitful, as preliminary results presented in Sect. 9.3 indicate. It would

also be desirable to compare results obtained by spectral methods with that obtained by other methods, as was done for the problem of rotating neutron stars (cf. Sect. 9.5) and extensively for hydrodynamical shocks [57].

In our opinion, one of the main advantage of spectral methods is that they allow a rigorous treatment of the regularity conditions associated with the singularities of spherical coordinates. This is important because spherical-like coordinates are obviously much more adapted than Cartesian coordinates for describing objects like stars or black holes. In particular, the number of points required to treat a star with Cartesian coordinates with a reasonable accuracy is considerably higher than that required by spherical coordinates. Moreover, the surface of the star (or the black hole horizon), where boundary conditions may have to be set, is described more simply with spherical coordinates, especially when surface-fitted spherical coordinates are introduced as in Sect. 7.4. Also the boundary conditions for Poisson-type equations are better expressed in spherical coordinates than in Cartesian ones.

We thank Prof. José-Maria Ibáñez and an anonymous referee for their carefull reading of the manuscript.

References

[1] A.M. Abrahams and J.W. York. 3+1 general relativity in hyperbolic form. In Marck and Lasota [38], pages 179–190.

[2] C. Basdevant, B. Legras, R. Sadourny, and M. Beland. A study of barotropic model flows: intermittency, waves and predictability. *J. Atmosph. Sciences*, 38:2305–2326, 1981.

[3] M. Bocquet, S. Bonazzola, E. Gourgoulhon, and J. Novak. Rotating neutron star models with a magnetic field. *Astron. & Astrophys.*, 301:757–775, 1995.

[4] S. Bonazzola, J. Frieben, and E. Gourgoulhon. Spontaneous symmetry breaking of rapidly rotating stars in general relativity. *Astrophys. J.*, 460:379–389, 1996.

[5] S. Bonazzola, J. Frieben, and E. Gourgoulhon. Spontaneous symmetry breaking of rapidly rotating stars in general relativity: influence of the 3d shift-vector. *Astron. & Astrophys.*, 331:280–290, 1998.

[6] S. Bonazzola, J. Frieben, E. Gourgoulhon, and J-A. Marck. Spectral methods in general relativity – toward the simulation of 3d-gravitational collapse of neutron stars. In A.V. Ilin and L.R. Scott, editors, *ICOSAHOM'95, Proc. of the Third International Conference on Spectral and High Order Methods (Houston, U.S.A., 5-9 June 1995)*, Houston Journal of Mathematics, pages 3–19, Houston, 1996. Houston Journal of Math.

[7] S. Bonazzola and E. Gourgoulhon. Gravitational waves from pulsars: emission by the magnetic-field-induced distortion. *Astron. & Astrophys.*, 312:675–690, 1996.

[8] S. Bonazzola and E. Gourgoulhon. Gravitational waves from accreting neutron stars. In I. Ciufolini and F. Fidecaro, editors, *Gravitational waves – sources and detectors*, pages 231–240, Singapore, 1997. World Scientific.

[9] S. Bonazzola and E. Gourgoulhon. Gravitational waves from neutron stars. In Marck and Lasota [38], pages 151–176.

[10] S Bonazzola, E. Gourgoulhon, P. Haensel, and J-A. Marck. Astrophysical sources of gravitational waves and neutrinos. In d'Inverno [20], pages 230–246.

[11] S. Bonazzola, E. Gourgoulhon, and J-A. Marck. Relativistic formalism to compute quasi-equilibrium configurations of non-synchronized neutron star binaries. *Phys. Rev. D*, 56:7740–7749, 1997.

[12] S. Bonazzola, E. Gourgoulhon, and J-A. Marck. Numerical approach for high precision 3-d relativistic star models. *Phys. Rev. D*, 58:104020, 1998.

[13] S. Bonazzola, E. Gourgoulhon, and J-A. Marck. Numerical models of irrotational binary neutron stars in general relativity. *Phys. Rev. Lett.*, submitted (preprint: gr-qc/9810072), 1998.

[14] S. Bonazzola, E. Gourgoulhon, M. Salgado, and J. A. Marck. Axisymmetric rotating relativistic bodies: a new numerical approach for "exact" solutions. *Astron. & Astrophys.*, 278:421–443, 1993.

[15] S. Bonazzola, J. Heyvaerts, and M. Perault. Jeans criterium in turbulent flows. *Astron. & Astrophys.*, 172:293–298, 1987.

[16] S. Bonazzola and J. A. Marck. 3d gas dynamics in a sphere. *J. of Comp. Phys.*, 87:201–230, 1990.

[17] S. Bonazzola and J-A. Marck. Efficiency of gravitational radiation from axisymmetric and 3d stellar collapse. i. polytropic case. *Astron. & Astrophys.*, 267:623–633, 1993.

[18] C. Canuto, M. Y. Hussaini, A. Quarteroni, and T. A. Zang. *Spectral methods in fluid dynamics*. Springer-Verlag, Berlin, 1988.

[19] B. Carter. Cosmic gamma ray bursts from black hole tidal disruption of stars ? *Astrophys. J.*, 391:L67–L70, 1992.

[20] R. A. d'Inverno, editor. *Approaches to numerical relativity*, Cambridge, England, 1992. Cambridge University Press.

[21] D. Gottlieb and S. A. Orszag. *Numerical analysis of spectral methods: theory and applications*. Society for Industrial and Applied Mathematics, Philadelphia, 1977.

[22] E. Gourgoulhon. Simple equations for general relativistic hydrodynamics in spherical symmetry applied to neutron star collapse. *Astron. & Astrophys.*, 252:651–663, 1991.

[23] E. Gourgoulhon. 1d numerical relativity applied to neutron star collapse. *Classical and Quantum Gravity*, 9:S117–S125, 1992.

[24] E. Gourgoulhon and S. Bonazzola. Noncircular axisymmetric stationary spacetimes. *Phys. Rev. D*, 48:2635–2652, 1993.

[25] E. Gourgoulhon and P. Haensel. Upper bounds on the neutrino burst from collapse of a neutron star into a black hole. *Astron. & Astrophys.*, 271:187–208, 1993.

[26] E. Gourgoulhon, P. Haensel, and D. Gondek. Maximum mass instability of neutron stars and weak interaction processes in dense matter. *Astron. & Astrophys.*, 294:747–756, 1995.

[27] J-O. Goussard, P. Haensel, and J.L. Zdunik. Rapid uniform rotation of protoneutron stars. *Astron. & Astrophys.*, 321:822–834, 1997.

[28] J-O. Goussard, P. Haensel, and J.L. Zdunik. Rapid differential rotation of protoneutron stars and constraints on radio pulsars periods. *Astron. & Astrophys.*, 330:1005–1016, 1998.

[29] D.S. Harned and D.D. Schnack. *J. of Comp. Phys.*, 65:57, 1986.

[30] B.K. Harrison, K.S. Thorne, M. Wakano, and J.A. Wheeler. *Gravitation theory and gravitational collapse*. Univers. Chicago Press, Chicago, 1965.

[31] J.M. Ibáñez, 1998. this volume.

[32] A. Kokhlov, I.D. Novikov, and C.J. Pethhick. Weak tidal encounter of a star with a massive black hole. *Astrophys. J.*, 432:163–178, 1993.

[33] C. Lanczos. *Applied Analysis*. Prentice-Hall, Englewood, N.J., 1956.

[34] J. Le Bourlot, G. Pineau des Forêts, E. Roueff, and D.R. Flower. Bistability in dark cloud chemistry. *Astrophys. J.*, 416:L87–L90, 1993.

[35] K. Lerbinger and J.F. Luciani. A new semi-implicit method for mhd computations. *J. of Comp. Phys.*, 97:444–459, 1991.

[36] Y. Maday, S. M. Ould Kaber, and E. Tadmor. *SIAM J. on Comp.*, 30:321, 1993.

[37] J-A. Marck and S. Bonazzola. Gravitational radiation from 3-d gravitational stellar core collapse. In d'Inverno [20], pages 247–257.

[38] J. A. Marck and J. P. Lasota, editors. *Relativistic Gravitation and Gravitational Radiation*, Cambridge, England, 1997. Cambridge University Press.

[39] J-A. Marck, A. Lioure, and S. Bonazzola. Numerical study of tidal interaction of a star and massive black hole. *Astron. & Astrophys.*, 306:666–674, 1996.

[40] J.M. Martí. High-order finite-difference schemes. In Marck and Lasota [38], pages 239–255.

[41] D.B. Melrose. *Non thermal process in diffuse magnetized plasma*, volume 1. Gordon & Breach, New-York, 1980.

[42] J. Novak. *Etude numérique de sources de rayonnement gravitationnel en théorie tenseur-scalaire*. PhD thesis, Université de Paris VII, 1998.

[43] J. Novak. Spherical neutron star collapse in tensor-scalar theory of gravity. *Phys. Rev. D*, 57:4789–4801, 1998.

[44] J. Novak. Neutron star transition to strong-scalar-field state in tensor-scalar gravity. *Phys. Rev. D*, 58:064019, 1998.

[45] T. Nozawa, N. Stergioulas, E. Gourgoulhon, and Y. Eriguchi. Construction of highly accurate models of rotating neutron stars — comparison of three different numerical schemes. *Astron. & Astrophys. Suppl. Ser.*, 132:431–454, 1998.

[46] J.R. Oppenheimer and G. Volkoff. On massive neutron cores. *Phys. Rev.*, 55:374–381, 1939.

[47] T. Passot, H. Politano, A. Pouquet, and P.L. Sulem. Subgrid-scale modeling in two-dimensional mhd turbulence. *Theor. Comp. Fluid Dyn.*, 1:47–60, 1990.

[48] T. Passot and A. Pouquet. Hyperviscosity for compressible flows using spectral methods. *J. of Comp. Phys.*, 75:300, 1988.

[49] T. Passot, E. Vasquez-Semadeni, and A. Pouquet. A turbulent model for the interstellar medium. ii. magnetic field and rotation. *Astrophys. J.*, 455:536–555, 1995.

[50] I.G. Petrovsky. *Lectures on partial differential equations*. Interscience, New-York, 1954.

[51] R.D. Richtmyer and K.W. Morton. *Difference methods for initial value problems*. Interscience, New-York, 1967.

[52] D.D. Schnack, D.C. Barnes, Z. Mikic, D.S. Harned, and E.J. Caramana. *J. of Comp. Phys.*, 70:330, 1987.

[53] L. Smarr and J.W. York. Radiation gauge in general relativity. *Phys. Rev. D*, 17:1945, 1978.

[54] E. Vasquez-Semadeni, T. Passot, and A. Pouquet. A turbulent model for the interstellar medium. i. treshold star formation and self-gravity. *Astrophys. J.*, 441:702–725, 1995.

[55] A. Vincent and M. Meneguzzi. The dynamics of the vorticity tubes in homogeneous turbulence. *J. Fluid Mech.*, 258:245–254, 1994.

[56] R.M. Wald. *General Relativity*. University of Chicago Press, Chicago, 1984.

[57] P. Woodward and P. Colella. The numerical simulation of two-dimensional fluid flow with strong shocks. *J. of Comp. Phys.*, 54:115–173, 1984.

[58] J.W. York. Role of conformal three-geometry in the dynamics of gravitation. *Phys. Rev. Lett.*, 28(16):1082–1085, 1972.

[59] J.W. York. Conformally invariant orthogonal decomposition of symmetric tensors on riemannian manifolds and the initial-value problem of general relativity. *J. of Math. Phys.*, 14(4):456–464, 1973.